Drought-Induced Epigenetic Memory in the cambium of Poplar Trees persists and primes future stress responses

Alexandre DUPLAN[1,2], Yu-Qi FENG[3], Gwenvaël LASKAR[1], Bao-Dong CAI[4], Vincent SEGURA[2,$], Alain DELAUNAY[1†], Isabelle LE JAN[1], Christian DAVIAUD[5], Anouar TOUMI[1], Francoise LAURANS[2], Mamadou Dia SOW[1,£], Odile ROGIER[2], Patrick POURSAT[6], Harold DURUFLÉ[2], Véronique JORGE[2], Leopoldo SANCHEZ[2], Hervé COCHARD[7], Isabel ALLONA[8,9], Jörg TOST[5], Régis FICHOT[1*], Stéphane MAURY[1*]

*corresponding authors: stephane.maury@univ-orleans.fr and regis.fichot@univ-orleans.fr

[1] P2e, Université d'Orléans, INRAE, EA 1207 USC 1328, 45067 Orléans, France.

[2] BioForA, INRAE, ONF, UMR 0588, 45075 Orléans, France.

[3] School of Bioengineering and Health, Wuhan Textile University, 430200 Wuhan, China.

[4] Wuhan Greensword Creation Technology Co. Ltd., Wuhan, China

[5] Laboratory for Epigenetics and Environment, Centre National de Recherche en Génomique Humaine, CEA - Institut de Biologie François Jacob, Université Paris Saclay, 91000 Evry, France.

[6] Unité Expérimentale GBFOr "Génétique et Biomasse Forestière" INRAE Centre de recherche Val de Loire site d'Ardon, 45075 Orléans, France.

[7] UMR-PIAF, INRAE, Université Clermont-Auvergne, 5 Chemin de Beaulieu, 63113 Clermont-Ferrand, France.

[8] Centro de Biotecnologıa y Genomica de Plantas, Universidad Politecnica de Madrid (UPM)–Instituto Nacional de Investigacion y Tecnologıa Agraria y Alimentaria (INIA-CSIC), Campus de Montegancedo UPM, Pozuelo de Alarcon, Madrid 28223, Spain.

[9] Departamento de Biotecnologıa-Biologıa Vegetal, Escuela Tecnica Superior de Ingenierıa Agronomica, Alimentaria y de Biosistemas, Universidad Politecnica de Madrid (UPM), Madrid 28040, Spain.

[†] Deceased 7 August 2024.

Present address:

[£] INRAE-UCA GDEC, 5 Chemin de Beaulieu, 63100, Clermont Ferrand, France.

[$] UMR AGAP Institut, Univ Montpellier, CIRAD, INRAE, Institut Agro Montpellier, 34398 Montpellier, France.

Abstract

Understanding how perennial plants such as trees perceive, integrate and memorize environmental stresses like water deficit is crucial in the context of climate change.

We investigated short-term and transannual memory of water deficit in cambium derived tissues of poplars (*Populus* spp.*)* using two contrasting genotypes and four genetically modified epitypes with altered DNA methylation machinery.

We found persistent changes in hormone profiles, gene expression and DNA methylation one week after stress relief, consistent with a molecular short-term stress memory. These signatures revealed distinct adaptive strategies between genotypes and marked variability between epitypes, demonstrating that both genetic and epigenetic backgrounds drive stress memory.

Trees already exposed to water deficit in Year 1 showed distinct physiological and molecular responses when subjected to a second water deficit in Year 2, supporting the persistence of a long-term trans-annual memory possibly involved in tree priming. The higher molecular plasticity observed in the intrinsically more sensitive genotype contrasted with the higher stability observed in the intrinsically more tolerant genotype. The number of memory genes was limited, but the results suggested that stable drought-induced DNA methylation changes, particularly in the CG context, contribute to long-term stress imprinting.

Our findings highlight the cambium as a reservoir for stress memory in trees and suggest that DNA methylation dynamics shaped by genetic predisposition, acting through cis- and trans-regulatory routes, may help fine-tuning growth *vs.* survival strategies across longer time frames. These insights open perspectives for harnessing epigenetic variation in tree breeding and management under increasing drought frequency.

KEYWORDS

DNA methylation, Phytohormones, *Populus*, Transcriptomic, Water deficit

Introduction

Trees, as sessile and perennial organisms, must continually adjust to environmental fluctuations to grow, reproduce, and survive. Acclimation, defined as phenotypic adjustment to changing conditions (i.e. plasticity; Nicotra et al., 2010, is critical for sustaining fitness across diverse environments. While genetic variation underlies much phenotypic diversity, recent research highlights the role of epigenetic mechanisms in shaping plant acclimation (Kakoulidou et al., 2021; Westerband et al., 2021). Epigenetics refers to heritable modifications in gene expression that occur without changes in the DNA sequence (Richards, 2006). In the context of climate change, such dynamic modifications are particularly relevant for long-lived species, where they may buffer variability across years and decades (Gallusci et al., 2023). They also offer applications for breeding and conservation of stress-resilient resources (Holeski et al., 2012; Plomion et al., 2018).

Among epigenetic marks, DNA methylation, especially cytosine methylation, is widely studied for its role in genome stability and transcriptional control (Mhiri et al., 2022; Muyle et al., 2022; Ramakrishnan et al., 2022). In plants, methylation occurs in CpG, CHG, and CHH contexts (H. Zhang et al., 2018). Its establishment relies on the RNA-directed DNA methylation (RdDM) pathway, in which small RNAs guide DRM2 (Domains Rearranged Methyltransferase 2) to specific loci for *de novo* methylation (Xie et al., 2025). Once established, methylation patterns are maintained through distinct, context-specific machinery: DRM2 and CMT3 preserve CHH and CHG methylation in euchromatin, while CMT2 and CMT3 act predominantly in heterochromatin. MET1 maintains CpG methylation with the help of the chromatin remodeler DDM1, which ensures access of methyltransferases to densely packed regions, whereas active DNA demethylation is carried out by ROS1 and DML enzymes (Xie et al., 2025). Following each round of DNA replication, these maintenance systems restore parental methylation patterns with remarkable precision. MET1 faithfully copies CpG methylation on the daughter strand, while CHG and CHH contexts depend on the recognition of histone H3K9me2 and siRNA-guided RdDM activity mediated by CMT2 and CMT3. This division of labor ensures high fidelity of CG methylation but more variable inheritance of non-CG methylation, contributing to the differential stability of epigenetic states within plant genomes. Promoter CpG and CHG/CHH methylation usually suppress transcription (Niederhuth et al., 2016; X. Zhang et al., 2006), whereas gene body CpG methylation stabilizes expression of housekeeping genes, protecting against aberrant transcription and TE insertions (Muyle et al., 2022). Overall, dynamic methylome modifications integrate both stability and flexibility, coordinating development and stress responses across timescales (Lloyd & Lister, 2022; Ramakrishnan et al., 2022). Moreover, DNA methylation constitutes a durable signature of chromatin state and offers indirect access to other epigenetic layers. Feedback loops connect CHG/CHH methylation with repressive marks like H3K9me2, while RdDM couples small RNAs, chromatin, and de novo methylation. Hence, methylome mapping reveals heritable transcriptional and chromatin states genome-wide, explaining its central role in plant epigenetics.

Water availability is a major factor of plant productivity and increasing drought frequency has been driving forest diebacks worldwide (Hammond et al., 2022). Severe drought can cause mortality through hydraulic failure and carbon imbalance (McDowell et al., 2022), while sublethal drought may leave persistent traces shaping future resistance, resilience, and

recovery (so-called ecological memory, Gessler et al., 2020). Stress memory in plants describes how prior exposure leaves molecular, physiological, or epigenetic imprints that modify subsequent responses (Crisp et al., 2016; Hilker et al., 2016). Memory occurs at multiple scales: within cells, tissues, or organisms (somatic memory), persisting from days to years, and across generations (Brenya et al., 2022; Farkas & Dobránszki, 2024; Gallusci et al., 2023). At the molecular level, it is supported by regulatory networks spanning genome, epigenome, proteome, and metabolome (Galviz et al., 2020; Harris et al., 2023).

Most mechanistic studies have focused on the annual *Arabidopsis thaliana*, mainly exploring short-term priming responses (Harris et al., 2023). Priming can be defined as the pre-conditioning by mild stress, chemical signals, or symbioses that enhances later responses (Lämke & Bäurle, 2017; Mauch-Mani et al., 2017). While *A. thaliana* has provided key insights (Kakoulidou et al., 2021), their relevance to long-lived trees is uncertain (Amaral et al., 2020; Gallusci et al., 2023). Perennials face recurrent stresses over decades, raising the question of how memory operates across short-term, transannual, and potentially transgenerational levels.

Previous studies in the model tree poplar have shown the existence of a drought-induced epigenetic memory in the shoot apical meristem (SAM), involving DNA methylation, hormonal and transcriptomic shifts (Lafon-Placette et al., 2018; Sow et al., 2021; Trontin et al., 2021). Such modifications may persist for months (A.-L. Le Gac et al., 2018) and transmit mitotically to developing leaves (A. laure Le Gac et al., 2019). The SAM has recently been identified as a hotspot of methylation dynamics and plasticity (Yang & Johannes, 2025), reinforcing its role as a memory reservoir. However, whether similar mechanisms operate in other meristems, for instance the vascular cambium that is responsible for radial growth, and how they may vary with genetic background remain largely unexplored.

Meristematic tissues are central to plasticity and potential memory. Persistent changes in transcription factors, metabolites, DNA methylation, and histone modifications have been observed during recovery (Crisp et al., 2016). Phytohormones, essential for stress responses and development (Zhao et al., 2021), also interact with chromatin regulation (Lafon-Placette et al., 2018; Liu et al., 2016; Ojolo et al., 2018; Peirats-Llobet et al., 2016; Yamamuro et al., 2016). This crosstalk is a key driver of acclimation (Maury et al., 2019). The vascular cambium is a particularly strong candidate for memory. This lateral meristem produces secondary xylem and phloem, responsible for radial growth, and remains active throughout life. Cambial initials integrate developmental and environmental signals, while their derivatives in wood and bark serve as long-term records (Maury et al., 2019). Hormonal gradients are known to be tightly regulated within the cambial zone (W. Ding et al., 2024; Fukuda, 2004; Mähönen et al., 2006; Nieminen et al., 2015; Planas-Riverola et al., 2019; Smetana et al., 2019) while epigenetic mechanisms including DNA methylation, histone variants and noncoding RNAs support cambial plasticity (Groover, 2025; Inácio et al., 2022). Water deficit may alter this balance, and recovery may involve active reprogramming. The altered epigenetic modifications and their potential persistence could thus provide an accessible tissue of choice to investigate cambial memory.

In this study, we investigated both short-term and transannual drought-induced epigenetic memory in cambium-derived tissues of poplar trees (*Populus* spp.). We combined the study of genetic influence by focusing on two *P. nigra* genotypes originating from distinct European populations (France *vs.* Italy) with the study of engineered epitypes of *P. tremula* × *P. alba* carrying altered expression of key methylation and demethylation factors (Xu & Law,

2024), including DDM1 (a chromatin remodeler) and DMLs (DNA demethylases) (Conde, 2017a, 2017b; Sow et al., 2021; Vigneaud et al., 2023; Zhu et al., 2013). We thus tested both genetic and epigenetic contributions to drought-induced memory. We combined ecophysiological characterization with hormone profiling, transcriptomics, and DNA methylation analyses of cambium-derived tissues. This multilayered approach disentangled physiological, genetic, and epigenetic contributions to memory across two timescales (one week *vs.* one year). Our central hypothesis was that the vascular cambium, as a meristem, functions as a reservoir of drought memory sustained through hormonal, transcriptional, and epigenetic changes, and that both genetic background and DNA methylation variation modulate its establishment and persistence. Overall, our work addresses how perennial meristems integrate environmental information, a fundamental question for understanding acclimation and resilience of forest trees under recurrent drought.

Materials and Methods

Plant material, growth conditions and experimental design

We conducted experiments on two *Populus nigra* L. genotypes (thereafter referred as *Pn* genotypes) and four *Populus tremula* L. × *Populus alba* L. (INRA 717-1B4) DNA methylation epitypes (thereafter referred as *Ptm* × *Pa* epitypes; see Table1 and Fig. 1). The *Pn* genotypes (Table 1) were chosen based on available plant material and data previously reported from a wide collection of 1160 cloned genotypes, originating from 14 natural populations across 11 river catchments in 4 European countries, installed in common gardens in France and Italy (more details on the origin of these genotypes are available in the GnpIS Information System (Steinbach et al., 2013). The *Ptm* × *Pa* epitypes were chosen based on previous experiments to include representative transgenic constructs affecting distinct methylation pathways (Table 1).

The experiment on *Pn* genotypes was initiated from homogeneous dormant cuttings sampled at the end of winter from current-year branches of trees growing at a nearby common garden. Cuttings were rooted in 10 L pots with a potting mix (Klassmann® RHP 25-564) complemented with Osmocote® PG Mix (1 kg/m^3 of N-P-K 80/35/60) and were grown in a heated greenhouse for two months under controlled conditions [photoperiod 16/8 (day/night, h), air temperature cycles 20/15 (day/night, °C) and daily PPFD of 950 µmol.m^{-2}.s^{-1}]. Early growing saplings were then transferred to an unheated greenhouse receiving natural daylight and following the course of the natural photoperiod until the end of the experiment in early September. The experiment on *Ptm* × *Pa* epitypes was initiated from *in vitro* micropropagated plantlets. Young acclimated plantlets were first rooted in 2 L pots before being transplanted in 10 L pots using the same soil substrate as for the *Pn* experiment. Plants were then grown in a GMO greenhouse under the same ambient conditions as for *Pn* genotypes.

Experiments on *Pn* and *Ptm* × *Pa* epitypes followed the same experimental design adapted from previous work (Sow et al., 2021). Treatments were initiated on 3-month-old plants and lasted for 6-weeks. Half of the plants were assigned to the well-watered treatment (Control, C) while the other half was assigned to a 5-week water deficit followed by a one-week rewatering (Stressed, S). Plants from the C treatment were maintained close to field capacity during the whole experiment using an automatic drip irrigation system connected to tensiometers (model INT4, Kriwan Industrie-Electronik GmbH, Germany). Plants from the S

treatment were maintained between 10 and 20% of soil relative extractable water (REW) based on daily individual measurements of soil water content (Bouyer et al., 2023; Sow et al., 2021) before being rewatered and maintained close to field capacity for one additional week before sampling (see sup. Fig. S1). The total number of plants amounted to 24 for *Pn* genotypes (2 treatments × 2 genotypes × 6 clonal replicates) and 48 for *Ptm* × *Pa* epitypes (2 treatments × 4 epitypes × 6 clonal replicates).

In order to explore the transannual epigenetic memory of the water deficit applied in Year 1, we decided to keep the *Pn* genotypes for one additional year (Year 2). We could not manage such exploratory experiments for the transgenic *Ptm* × *Pa* epitypes because of technical limitations of keeping our transgenic trees in the GMO greenhouse for over a year. In Year 2, half of the C plants from Year 1 were assigned to the control well-watered treatment (C/C) or the water deficit treatment followed by rewatering (C/S), while half of the S plants subjected to water deficit in Year 1 (S) were similarly assigned either to the control well-watered treatment (S/C) or the water deficit treatment followed by rewatering (S/S). The treatments applied and the methods used in Year 2 were identical to Year 1. (Fig. 1).

Plant-level physiological monitoring

Physiological monitoring concentrated on the core experiments conducted in Year 1 on both *Pn* genotypes and *Ptm* × *Pa* epitypes (see below and Fig. 1). Measurements in Year 2 (transannual memory in *Pn* genotypes) were restricted to soil water status and growth.

Tree growth was monitored during the course of the experiment by measuring stem height and diameter of all plants every two to three days. Leaf net assimilation rate (A_{net}) and stomatal conductance to water vapour (g_s) were assessed 8-9 times throughout the experiment to evaluate the effects of water deficit on leaf gas exchange physiology (n = 3 random replicates per genotype/epitype per treatment at each date). Measurements were performed on fully mature leaves in the top third of the plants using a Li-6400 open path portable photosynthesis system (Li-Cor, Lincoln, NE, USA) equipped with a LED light source (Li-6400-02B) under saturating chamber conditions (photosynthetic photon flux density of 1500 $\mu mol.m^{-2}.s^{-1}$, ambient CO_2 concentration of 400 ppm and reference vapour pressure deficit maintained close to 1 kPa). Leaf-level intrinsic water-use efficiency ($_i$WUE) was computed directly from instantaneous leaf gas exchange as the ratio between A_{net} and g_s and assessed retrospectively by measuring bulk leaf carbon isotope composition ($\delta^{13}C_{leaf}$) on mature leaves formed during the 5-week water deficit period. We also measured daily minimum leaf water potential ($\Psi_{leaf-min}$) repeatedly during the course of the experiment (n = 3 random replicates per genotype/epitype per treatment at each date) to assess differences in water relations. Finally, we evaluated xylem resistance to drought-induced embolism in order to evaluate intrinsic resistance to drought-induced hydraulic dysfunction (Fichot et al., 2015). Measurements were performed at the end of the experiment on stems of all well-watered control plants (n = 6 per genotype/epitype) using the cavitron centrifugation technique Cochard et al., 2005.

Sampling of cambium derived tissues

Tissue sampling for molecular analyses was performed in Year 1 (*Pn* genotypes and *Ptm* × *Pa* epitypes, short-term memory) and in Year 2 (*Pn* genotypes, transannual memory) at the end of the 1-week rewatering following water deficit (n = 3 replicates per genotype/epitype per treatment) (see Fig. 1). We sampled approximately 80 cm-long stem sections starting at 20 cm

above the ground (Chateigner et al., 2020). The bark was split using a sterile scalpel and manually detached from the stem before gently scratching tissues on both sides (bark *vs*. stem) thus leading to two distinct tissue fractions. Histological analyses showed that the tissue fraction from the stem side mostly corresponded to young differentiating secondary xylem while the tissue fraction from the bark side contained most of the cambial cells and secondary phloem derivatives (Fig. S2). Sampled tissue fractions were immediately hand-ground in liquid nitrogen using pestles and mortars and stored separately at -80°C pending further milling and individual extraction of genomic DNA and RNA.

Phytohormone quantification

Phytohormones in cambium-derived tissues (*n* = 3 replicates per genotype/epitype per treatment) were quantified from 20 mg dry powder from pooled tissue fractions using the LC-MS technique (Thermo Scientific Ultimate 3000 UHPLC coupled with a TSQ Quantiva, Waltham, Massachusetts, USA). The following 15 phytohormones were analysed: Auxin (IAA), Abscisic Acid (ABA), 4'-dihydrophaseic acid (DPA; ABA derivative), Jasmonic acid (JA), 12-oxo-phytodienoic acid (OPDA, JA derivative), Salicylic Acid (SA), *cis*-Zeatin-O-glucoside Cytokinin (cZOG), Isopentenyl adenine riboside Cytokinin (iPR), *cis*- or *trans*-Zeatin riboside Cytokinin (cZR or tZR), Gibberellins (GA8, GA12, GA19), castasterone (CS), 6-Deoxocastasterone (6-deoxoCS).

For GA analysis, samples were extracted with 1 mL 80% (v/v) methanol. [$^2H_2$] GA1, [$^2H_2$] GA3, [$^2H_2$] GA4, [$^2H_2$] GA5, [$^2H_2$] GA6, [$^2H_2$] GA7, [$^2H_2$] GA8, [$^2H_2$], [$^2H_2$] GA12, [$^2H_2$] GA15, [$^2H_2$] GA19, [$^2H_2$] GA20, [$^2H_2$] GA24, [$^2H_2$] GA34, [$^2H_2$] GA44, [$^2H_2$] GA51 and [$^2H_2$] GA53 were added to plant samples as internal standards for quantification. The samples were extracted at 4°C for 12 h. The analysis of GA content was performed after sample pretreatment Chen et al., 2012. For brassinosteroids (BR) analysis, samples were extracted with 1 mL acetonitrile. Then [$^2H_3$]BL, [$^2H_3$]CS, [$^2H_3$]6-deoxoCS were added as internal standards for quantification. The samples were extracted at 4°C for 12 h. The analysis of BR content was performed after sample pretreatment (J. Ding et al., 2013). Finally, for IAA, ABA, JA, SA and cytokinins (CK), samples were extracted with 1 mL acetonitrile. Then [$^2H_2$]IAA, [$^2H_6$]ABA, [$^2H_3$]PA, [$^2H_3$]DPA, [$^2H_3$]ABAGE, [$^2H_4$]7′-OH-ABA, [$^2H_3$]neoPA, [$^2H_4$]SA, [$^2H_6$]iP, [$^2H_6$]iPR, [$^2H_6$]iP9G, [$^2H_5$]tZ, [$^2H_5$]tZR, [$^2H_5$]tZ7G, [$^2H_5$]tZ9G, [$^2H_5$] tZOG, [$^{15}N_4$]cZ, [$^2H_3$]DHZ, [$^2H_3$]DHZR, [$^2H_3$]DHZ9G, [$^2H_7$]DHZOG were added as internal standard for quantification. The samples were extracted at 4°C for 12 h. The analysis was performed after sample pretreatment (Cai et al., 2015).

Transcriptome

Total RNA was extracted from each tissue fraction independently (stem *vs*. bark) for each tree with the RNeasy Plant kit and following the manufacturer's recommendations (Qiagen, France). Extracted RNAs were then treated with DNase I to ensure the elimination of genomic DNA. RNAs were quantified with a Nanodrop spectrometer after being eluted in RNAse-DNAse free water. RNAs were further analysed for DNA contamination and RNA integrity with RNA integrity number (RIN) measurements using a Bioanalyzer 2100 (Agilent Technologies). RNAs from the two independent tissue fractions of the same individual were

finally pooled in an equimolar extract before sequencing (Chateigner et al., 2020). We thus considered the pooled extracts to be representative of cambial cells plus secondary xylem and phloem derivatives, respectively, in equivalent proportions.

Ribosomal RNA depletion (NEBNext® rRNA Depletion Kit v2, New England Biolabs) were realised by the IGen Seq platform (ICM, Paris, France) with 300 ng input total RNA. RNA library preparation was realised following the manufacturer's recommendations (NEBNext® Ultra™ II Directional RNA Library Prep Kit for Illumina, New England Biolabs) and sequenced in paired end mode on an Illumina Novaseq 6000 (San Diego, CA, USA), corresponding to 2x85 Millions 100 base pair reads per sample after demultiplexing. The manufacturer's pipeline software was used to generate FASTQ sequence files.

To analyse the transcriptomic data, a RNA-seq bioinformatic workflow on the Galaxy instance of the Interactions Hôtes Pathogènes Environnements (IHPE; http://galaxy.univ-perp.fr/ (Perpignan, France); https://bioinfo.univ-perp.fr/) was developed. The data were filtered using TrimGalore v0.6.3 (Krueger et al., 2023) with a quality threshold of Q20. Reads were mapped to the *Populus trichocarpa* V4.1 genome (Phytozome version V4.1) using Bowtie2 v2.3.4.3 (Conde et al., 2017) with the following options: D 10, R 2, L 22 and -i S,0,2.50.

We used the Salmon quasi-mapping tool v1.5.1 (Patro et al., 2017) to quantify the number of aligned reads per gene and per transcript with the options k 21, seqBias and gcBias. Differentially expressed transcripts (DETs) were identified using the bioconductor R package DESeq2 v2.11.40.7 (Love et al., 2014). Read count matrices generated using Salmon were used as input for DESeq2. To optimise the search for low expressed genes in our samples, we set a low transcripts per million (TPM) detection threshold at 0.1, retaining genes with expression of at least TPM ≥ 0.1 in at least one triplicate sample. Following Benjamini-Hochberg correction, genes and transcripts with an adjusted $p-$value ≤ 0.05 and log2-fold changes ≤ -0.5 or ≥ 0.5 were considered as differentially expressed.

We analysed alternative splicing (AS) on the RNA-seq data using both rMATS v4.0.2 (S. Shen et al., 2014) and SUPPA v2.0 (Trincado et al., 2018) in collaboration with the IGen Seq platform (ICM, Paris, France). An alignment was performed with the STAR v2.5.3 tool (Dobin et al., 2013) on the *Populus trichocarpa* genome (version V4.1). Then, rMATS software was used for AS analysis with the following parameters: readLength 101, cstat 0.0001. For SUPPA2, the parameters followed the recommended procedure available at https://github.com/comprna/SUPPA/wiki/SUPPA2-tutorial. Differential splicing events (DSE) were classified various types of alternative splicing events detected including skipped exons (SE), alternative 3' splice sites (A3SS), alternative 5' splice sites (A5SS), mutually exclusive exons (MX), retained introns (RI), alternative first exons (AF), and alternative last exons (AL).

Methylome

The procedure has previously been described in detail (Sow et al., 2023). Briefly, genomic DNA (gDNA) was extracted using cetyltrimethylammonium bromide (CTAB) extraction buffer (Doyle & Doyle, 1987; Sow et al., 2021). Extracted gDNA was quantified using a Nanodrop spectrometer (Thermo Fisher Scientific, Waltham, MA, USA). An equimolar pool of 2 µg DNA at 100 ng.µL^{-1} was then prepared for each treatment and genotype/epitype from the gDNA samples of the three individual replicates and the 2 tissue fractions (see above). The

gDNA pools were then used for whole genome bisulfite sequencing (WGBS) using the Ultralow Methyl-Seq System (Tecan Genomics) (CEA laboratory, CNRGH, Evry, France) (Dugé de Bernonville et al., 2022; Sow et al., 2021, 2023; Vigneaud et al., 2023). The sequencing was performed in paired-end mode (2×150bp) on an Illumina HiSeq4000 platform, aiming for a coverage of 40X. The raw data were saved as FASTQ files.

For methylome analysis, we used the previously reported bioinformatic workflow (Dugé de Bernonville et al., 2022; Sow et al., 2021, 2023; Vigneaud et al., 2023). Differentially methylated cytosines (DMCs) were identified with the methylKit R package (Akalin et al., 2012) with a minimum coverage of 10X, a methylation difference of at least 5% for the three contexts and *q*-value ≤ 0.05 (Dugé de Bernonville et al., 2022; Vigneaud et al., 2023). Differentially methylated genes (DMG) or transposable elements (DMTE) were defined as gene or TE sequences, respectively, containing at least one DMC. Identified genes were annotated according to the reference genome *P. trichocarpa* V.4.1. Gene Ontology (GO) enrichment was performed using *A. thaliana* orthologs of detected genes using Metascape v3.5 (Y. Zhou et al., 2019), using default parameters. *p-values* were computed with a hypergeometric test and the Benjamini-Hochberg correction was used for the correction of multiple-testing.

Statistical analysis

Exploration and statistical analyses of physiological data were carried out using the R software (R Core Team https://doi.org/10.59350/t79xt-tf203). All tests were considered significant at $P < 0.05$. Vulnerability curves relating xylem water potential to the percent loss of xylem hydraulic conductance were processed using the R *fitplc* package (Duursma & Choat, 2017) to estimate the water potential generating 50% of embolism (P_{50}). Differences between treatments or genotypes/epitypes were tested for all traits using analysis of variance followed by Tukey's HSD post-hoc test in case of significant differences.

Results

Growth and water relations

General patterns for soil REW, growth and physiological traits in Year 1 were similar between *Pn* genotypes and *Ptm* × *Pa* epitypes (Fig. 2, Fig. S1), indicating that although performed independently, experiments were comparable in terms of treatment intensity and general effects on plant physiology. For all genotypes/epitypes, water deficit induced significant growth reductions and changes in leaf physiology (Fig. 2, Fig. S1). Height growth remained steady, although lower than controls, throughout the experiment (Fig. S1). Radial growth seriously inflected after 20 days of water deficit but in most cases did not cease completely (Fig. S1).

In *Pn* genotypes, PG-31 displayed overall faster growth than DRA-038, especially radial growth under water deficit, and showed significantly higher tolerance to embolism (i.e. lower P_{50}) (Fig. 2A). $\Psi_{min\text{-}leaf}$ remained high and comparable across genotypes and treatments (-1.25 ± 0.06 MPa on average) suggesting comparable isohydric behaviours. In addition, the two genotypes did not differ significantly in leaf physiological traits and responded similarly to water deficit (Fig. 2A). Based on these observations, PG-31 was considered to be intrinsically more tolerant to water deficit than DRA-038.

Ptm × *Pa* epitypes did not differ significantly in height growth regardless of the treatment while differences were more apparent for radial growth (Fig. 2B). Under control conditions, OX-*dml* showed the fastest radial growth while RNAi-*ddm1* was the slowest (Fig. 2B); under water deficit conditions, differences were not significant, probably because of the important growth reductions observed in all lines, but modified lines all tended to show superior radial growth than the WT with OX-*dml* still showing the fastest growth (Fig. 2B). OX-*dml* was also significantly more tolerant to drought-induced embolism (Fig. 2B). $\Psi_{min\text{-}leaf}$ remained comparable between epitypes, but was slightly reduced in response to water deficit (-0.78 ± 0.04 MPa vs. -0.99 ± 0.04 MPa, respectively, $P < 0.001$) suggesting a slightly less isohydric behaviour of *Ptm* × *Pa* epitypes compared to *Pn* genotypes. Leaf traits were not significantly different between epitypes, except for g_s of RNAi-*ddm1* under control conditions, and showed similar variations in response to water deficit. Based on these observations, OX-*dml* was considered to be the most intrinsically tolerant epitype to water deficit.

We repeated the water deficit experiment in Year 2 on the two *Pn* genotypes to explore stress memory and potential priming. Saplings that experienced water deficit in Year 1 and maintained under control conditions in Year 2 (S/C) exhibited lower growth than saplings from the C/C control treatment in the genotype DRA-038 (Fig. 3), suggesting a legacy effect of water deficit on growth in Year 2 at least in this genotype. In contrast, the growth of saplings that experienced water deficit the two consecutive years (S/S) was not impaired compared to saplings that only experienced water deficit in Year 2 (C/S) in both genotypes (Fig. 3), suggesting that the negative legacy effect of water deficit on growth possibly inherited from Year 1 (see above for DRA-038) was not additive under a repeated stress.

Hormonal balance in Cambium-Derived Tissues

Concentrations of 15 phytohormonal compounds were measured in the cambium-derived tissues by LC-MS (Fig. 4). For the *Pn* genotypes, principal component analysis (PCA) revealed that the first three components explained 83.8% of the total variance with principal component (PC) 1 (39.9% of the variance) strongly positively associated with CS, DPA, cZR and GA19 and negatively with JA (Fig. 4A). The PC2 (29.5% of the variance) was mostly positively associated with cZOG and SA and negatively to GA12 (Fig. 4A). PC3 explained 14.4% of the variation, with 6-deoxoCS, tZR, JA, and ABA contributing the most (Fig_S3). Projection of individuals onto the principal plane (Fig. 4B) clearly differentiated genotypes, treatments and years. Genotype DRA-038 was overall more responsive than PG-31, (12/15 hormones significantly different between treatments vs. 9/15 in Year 1; 15/15 vs. 8/15 in Year 2) (Fig. 4E and Sup_table_1). In Year 1 (S vs. C), common responses (i.e. in the same direction) across genotypes were observed for ABA, JA, cZOG, tZR, GA12, and GA19 while opposite responses (i.e. in opposite direction) could be observed for CS (Fig. 4E, Sup_table_1). In Year 2 (S/S vs. C/S), common responses across genotypes were observed for JA, OPDA, iPR, and GA19 while opposite responses could be observed for SA, cZOG, tZR and GA12 (Fig. 4E, Sup_table_1). In addition, the comparison of S *vs*. C patterns (Year 1) with C/S *vs*. S/S patterns (Year 2) revealed a few opposite switches between years for DRA-038 (tZR, cZR and GA19) or PG-31 (cZOG, GA12 and GA19) (Fig. 4E, Sup_table_1).

For the *Ptm* × *Pa* epitypes, PCA revealed that the first three components explained 76.6% of the total variance with PC1 (42.6% of the variance) positively associated with GA19, ABA, DPA, IAA, and JA and negatively with OPDA and cZOG Fig. 4C). PC2 (18.8%

variance) was associated positively with 6-deoxoCS, GA12, and SA and negatively with tZR (Fig. 4C). PC3 explained 15.2% of the variation, with iPR and cZR contributing most (Fig_S4). Projection of individuals onto the first PCs clearly differentiated epitypes and treatments (Fig. 4D). While epitypes showed distinct projections in control conditions, they tended to group together in stressed conditions, with the exception of OX-*dml*. About half of the compounds (7/15) showed common responses to water deficit among the epitypes (IAA, ABA, DPA, OPDA, cZOG, GA 19 and CS) (Fig. 4E), while the other half showed epitype-specific or non-significant changes. The most notable changes for each epitype (vs. WT) were higher contents in gibberellins (GA8 and GA19) and lower content in cytokinin (tZR) for OX-*dml*, variable amounts of cytokinins for RNAi-*dml*, higher amounts of CS and lower amounts of ABA and GA19 for RNAi- *ddm1* (Fig_S5).

Among all genotypes and epitypes, ABA and JA consistently decreased in response to water deficit, indicating a common signature across genetic backgrounds (Fig. 4E). Quantitatively, the main discriminator between genotypes and epitypes was the baseline level of DPA, which was ~10-fold higher in *Pn* genotypes compared to *Ptm* × *Pa* epitypes (Sup_table_1).

Transcriptome analysis

Differentially expressed transcripts (DETs)

In *Pn* genotypes, 54% to 70% of the 52,000 annotated poplar transcripts were detected across conditions and years, with the highest proportion observed in DRA-038 under the C/S treatment in Year 2 (Fig_S6, Fig. 5A, 5B). In Year 1, 292 and 122 DETs were observed between C and S treatments in DRA-038 and PG-31, respectively (Fig. 5A). In Year 2, we found 141 and 136 DETs between C/S and S/S treatments in DRA-038 and PG-31, respectively (Fig. 5A, 5C). Functional annotation revealed that DETs in Year 1 in both genotypes mainly involved metabolic and developmental processes and phosphatidylinositol signalling (Fig. 5B). In Year 2, PG-31 displayed additional tags related to cambium activity and epigenetic regulation (Fig. 5B).

In Year 1, only 8 DETs were shared between DRA-038 and PG-31 (Fig. 5C; Table 2) and were associated with stress and hormonal pathways, including two *UMAMIT* amino acid transporters (salicylic acid pathway), *EIF2-GAMMA* (stress-associated translation initiation), *CYP83A1* (auxin-related metabolism), and two alternative splicing events (ASE) of *CP29A* (chloroplast RNA splicing, ABA/cold response) (Sup_table_2). In Year 2, only three DETs were shared between DRA-038 and PG-31, including an Rcd1-like protein (NOT9a), a regulator of both developmental and stress responses through regulation of gene expression by RNA-induced silencing complex (RISC) (Fig. 5C; Table 2; Sup_table_2). Finally, only a small number of DETs were shared between Year 1 (S vs. C) and Year 2 (C/S vs. S/S): six in DRA-038 and two in PG-31 (Fig. 5C; Table 2). These transannual DETs were involved in abiotic stress responses, vascular meristem development, and hormonal (auxin and jasmonic acid; Sup_table_2) signalling. Interestingly, the DETs conserved across years in PG-31 showed enhanced responses in Year 2, whereas those in DRA-038 exhibited variable patterns in direction and/or magnitude (Fig. 5C).

The number of genotypic DETs (DRA-038 vs. PG-31) varied from 297 (Year 2 in S/S condition) to 1930 (Year 1 in S condition) depending on treatments and years (Fig_S7). 254 genotypic DETs were conserved between C (Year 1) and C/S (Year 2) treatments, all with a comparable expression pattern (up or down-regulated) except one (AMP-dependent synthetase

and ligase *Potri.017G138350*); 168 genotypic DETs were conserved between S (Year 1) and S/S (Year 2) treatments, all with a comparable expression pattern.

The majority of Differentially Spliced Events (DSEs) were genotype-specific (Fig_S8), with a conservation of 21 DSEs in PG-31 between Year 1 and Year 2. Across *Pn* genotypes, 351 stress-induced and 287 genotype-specific DSEs (mostly A3SS, SE, and A5SS types; Fig_S9 A; see materials and methods for DSE classification) were detected, representing a small fraction of the known poplar DSEs (over 9 000 presents in the reference genome *P. trichocarpa* V4.1). Only nine overlapped with DETs, six of which were involved in chromatin remodelling and hormone (Auxin and JA) signalling pathways (Table 2; Sup_Table_2).

In *Ptm* × *Pa* epitypes, transcript detection ranged from 16189 (OX-*dml*, S condition) to 28883 (OX-*dml*, C condition) (Fig. 6A, Fig_S6, Fig_S11). Differential expression analysis revealed from 98 (RNAi-*ddm1*) to 415 (WT) DETs in response to water deficit (Fig. 6A), with 46 overlapping with those detected in *Pn* genotypes (Fig_S12). Most stress-induced DETs were line-specific and related to cell wall modification or growth processes (Fig. 6B, Fig_S10). The OX-*dml* line showed more up-regulated DETs and specific enrichment for "response to water deprivation", “auxin transport” and "response to gibberellins" (Fig. 6A, 6B).

To identify stress-responsive signatures across epitypes, we focused on stress-induced DETs shared by at least two lines, thereby identifying 46 genes involved in transcriptional regulation, auxin response, and xylem development (Fig. 6C; Sup_table_3). Three expression clusters could be observed: (I) downregulated DETs in WT, (II) upregulated DETs in WT, and (III) DETs uniquely regulated in modified lines. Notably, *dml*-affected lines (OX-*dml*, RNAi-*dml*) often exhibited reversed expression patterns compared to WT (clusters I and II; Fig. 6C).

Line-specific comparisons to WT under C and S conditions identified 137 (RNAi-*ddm1*, C condition) to 1 999 (RNAi-*dml*, C condition) DETs depending on the line (Fig_S13, Fig_S14). Among DETs shared across epitypes, only 20 DETs showed opposite expressions (Fig. 6D). For example, *RAF24* (osmotic stress response) was upregulated in OX-*dml* but downregulated in RNAi-*ddm1*, while *ILITHYIA* (developmental regulation) showed opposite expression between RNAi-*dml* and OX-*dml* under stress (Fig. 6D). Under S conditions, OX-*dml* exhibited a higher proportion of upregulated DETs, including three highly induced genes of unknown function on chromosome 8 (*Potri.008G224111.2*, *Potri.008G224147.1*, *Potri.008G224219.1*).

While the majority of DSEs were epitype-specific (Fig_S8) with 257 DSEs detected (Fig_S8, Fig_S9 A), of which 12 and 30 were also classified as DETs, we could also detect 181 stress-induced DSEs. GO enrichment analysis shows genes related to "positive regulation of reproductive processes", including several developmental transcription factors involved in developmental or hormonal signalling (Sup_Table_5 and Fig_S9 B).

Methylome analysis

Variation in methylation contexts

In *Pn* genotypes, stress-induced DMCs were primarily found in the CG context, followed by CHG and CHH, with overall a balanced proportion of hyper- and hypomethylation (Fig. 7A). PG-31 showed a markedly higher number of DMCs compared to DRA-038, although DRA-038 showed the strongest relative increase in CG DMCs from Year 1 to Year 2 (22-fold) (Fig. 7A).

We compared the DMCs identified in the two *Pn* genotypes under controlled

greenhouse conditions (present study) with DMCs identified in the same two genotypes but grown in an outdoor common garden (Sow et al., 2023) (Fig. 7B). Environmentally-induced DMCs (greenhouse vs. common garden) were predominantly found in the CHH context (up to 248 000), with partial conservation (45-65%) across genotypes (Fig. 7B; Fig_S15). In contrast, genotype-specific DMCs (PG-31 versus DRA-038) were mainly found in CG (up to 490 000) compared to CHG and CHH contexts and showed low conservation (<5% for the 3 contexts) across growing environments, highlighting strong genotype-by-environment interactions (Fig. 7B; Fig_S15).

In *Ptm* × *Pa* epitypes, stress-induced DMCs were predominantly found in CHH and were mostly (>97%) hypermethylated (Fig. 7C). RNAi-*ddm1* differed from other lines by presenting more DMCs in CG and a relatively more balanced proportion of hyper- and hypomethylation. Line-specific DMCs (i.e. comparison to WT) were 10–30 times more abundant than stress-induced DMCs especially in RNAi-*ddm1* and were primarily found in CG except for the RNAi-*ddm1* line showing more DMCs in CHG (Fig. 7D).

Methylation Changes in Genes and Transposable Elements

In *Pn* genotypes, 15.8 (Year 2) to 33.4 % (Year 1) of stress-related DMCs were localized in TEs (Differentially methylated TE or DMTEs) (Fig. 8A). These DMTEs were genotype-specific (Fig_S16): PG-31 showed high hypermethylation of TEs under stress compared to DRA-038 (Fig. 8B). 46.3% to 61.3% of stress-induced DMCs were localized to genes (thereafter called Differentially Methylated Genes or DMGs), particularly exons (Fig. 8A, Fig_S17). The number of DMGs ranged from 221 (DRA-038, Year 1) to 4,523 (PG-31, Year 2) (Fig_S18). Functional enrichment of DMGs revealed general categories related to metabolism (such as ATP dependent activity and catalytic activity) (Fig_S19). Shared DMGs between genotypes increased markedly from Year 1 (19 genes) to Year 2 (1 119 genes) (Fig_S18). Across genotypes and years, most DETs showed no DMCs (Fig. 6C); the few DETs showing DMCs were mostly found in Year 2 and belonged to the ON/OFF category (24 for DRA-038 and 30 for PG-31) (Fig. 8C, see also Fig. 5C).

In genotype DRA-038 during the second year, several DETs belonging to the ON/OFF category also exhibited DMCs located within or near their gene bodies. These genes include *Potri.005G182100* (histone methyltransferase H3-K4 specific) and *Potri.017G070500* (*5′-3′* exonuclease family protein), both showing evidence of alternative splicing between isoforms with opposite expression patterns; with *Potri.005G182100.1* and *Potri.017G070500.1* being down-regulated, while *Potri.005G182100.4* and *Potri.017G070500.2* were up-regulated. both showing evidence of alternative splicing between isoforms with opposite expression patterns; with *Potri.005G182100.1* and *Potri.017G070500.1* being down-regulated, while *Potri.005G182100.4* and *Potri.017G070500.2* were up-regulated.

In *Ptm* × *Pa* epitypes, stress-induced DMCs were mainly found in TEs (65.9%), particularly in LTR-Gypsy and Copia elements, and were mostly hypermethylated (Fig. 8A and 8D, Fig_S16, Fig_S20). 16.5 % of stress-induced DMCs were localized in genes found to be involved in ATP-dependent activity, gene expression, cellular localisation (Fig_S21). A low number of these stress-induced DMGs (3 in RNAi-*dml* to 19 in WT) overlapped with DETs (Fig_S18) (Fig. 8E). In contrast, line-specific DMTEs, which were particularly abundant in RNAi-*ddm1*, were predominantly hypomethylated (Fig. 8F). In addition, the majority (50–70%) of line-specific DETs corresponded to DMGs (Fig. 8G). For example, functional enrichment for the OX-*dml* line, showed regulation of cellular or metabolic processes and

epigenetic regulation of gene expression for the ON/OFF DET-DMG category (324 genes; Fig_S22), while the quantitatively expressed DET-DMGs showed metabolic or cellular processes and regulatory ncRNA processing (701 genes; Fig_S22).

Finally, no direct association was found between stress-induced DMCs and DSE (Fig_S23). However, over 78% of genotype- and epitype-specific DSE overlapped with DMCs (Fig_S24 A). GO enrichment pointed to 'chromatin remodeling' as the top term (Fig_S24 B). Finally, the gene *Potri.019G052500*, containing the most DMCs (314), exhibited a switch from hypo- to hypermethylation at a spliced exon (Fig_S24 C).

Discussion

Previous studies in *Populus* demonstrated that water deficit induces persistent molecular changes in shoot apical meristems (SAMs) that remain detectable after one week of recovery (Lafon-Placette et al., 2018; A.-L. Le Gac et al., 2018; Sow et al., 2021), in line with the concept of short-term somatic stress memory (Crisp et al., 2016; Hilker et al., 2016). Our work extends this perspective to the vascular cambium, the meristematic tissue responsible for radial growth and wood formation, a likely reservoir for long-term epigenetic imprinting (Maury et al., 2019). Most importantly, we identified a few molecular changes that persisted one year later in trees subjected to a second water deficit, suggesting a stable epigenetic memory that could prime future drought responses. Whether this transannual memory does confer priming remains to be elucidated, but the tissue specificity and molecular depth underscore its central role in orienting stress-induced acclimation in the vascular cambium.

---

1. Cambium-derived tissues retain drought-associated molecular signatures consistent with a short-term somatic memory

The prolonged exposure to five weeks of water deficit significantly altered tree carbon and water relations. This was supported by a marked reduction in stomatal conductance, enhanced water-use efficiency, and most importantly decrease in primary and secondary growth, but without complete growth cessation. Stress intensity was thus moderate and allowed a progressive recovery within one week of rewatering.

Hormonal profiles retained clear stress-induced imprints. Drought exposure decreased ABA, JA, and IAA levels, while increasing brassinosteroids (BRs) and GA_{12} across all genotypes and epitypes. The persistence of reduced ABA levels, a hallmark stress hormone, indicated growth recovery rather than ongoing stress signaling (Kuromori et al., 2018; Tong et al., 2014), consistent with a short-term molecular memory during post-stress recovery (Crisp et al., 2016; Hilker et al., 2016). It is worth noting, however, that hormone contents as measured in our study most likely included distinct pools from both xylem and phloem derivatives, some acting locally but others possibly transported to vascular tissues at the time of sampling; they are thus best interpreted as a global post-stress signature rather than an entirely local meristematic signal. Still, the main hormones cited above were concordant in a

context of cambial growth. IAA is known to accumulate toward the xylem to promote differentiation (Ruzicka et al., 2015; Smetana et al., 2019), cytokinins stimulate phloem identity (Mähönen et al., 2006), while BRs and GAs synergize with auxin to expand xylem (Planas-Riverola et al., 2019). ABA and JA, in contrast, generally restrict cambial activity and slow growth (Fukuda, 2004; Nieminen et al., 2008).

The transcriptomic analysis confirmed a selective molecular reprogramming following the release of water deficit. Approximately 0.2% of the transcriptome (200–250 genes) was differentially expressed, contrasting with the extensive transcriptomic responses typically reported during acute drought stress (Cohen et al., 2010; Wilkins et al., 2009), but in line with previous findings in poplar SAMs following rewatering (Lafon-Placette et al., 2018; Sow et al., 2021). DETs were enriched in cell wall organization, hormone pathways and signaling processes, consistent with an active remodeling related to growth resumption. The persistence of such signals one week after rewatering thus also supports the existence of a short-term molecular memory (Crisp et al., 2016; Hilker et al., 2016).

At the epigenetic level, thousands of DMCs were detected in the three methylation contexts despite specific patterns between *P. nigra* genotypes and *P. tremula* × *P. alba* epitypes (see discussion below). Methylation in CG and CHG is generally linked to stable expression states, whereas CHH methylation is often more transient, stress-responsive, and coupled to transposable element activity (Dowen et al., 2012; Talarico et al., 2024). As these signatures persisted in cambial tissues upon rewatering, they may not only reflect a transient stress footprint, but may have contributed to the establishment of a short-term molecular memory of drought stress. Only a small subset of DETs (up to 22) actually overlapped with nearby DMCs, but these included genes spanning different molecular functions, with notable candidates such as ERD family proteins, involved in early responses to dehydration (Alves et al., 2011), and UBP13, a regulator of plant development and stress that modulates MYC2 levels in jasmonate signaling (S. Zhang et al., 2024). Although limited in number, such overlap points to a potential cross-talk between epigenetic regulation and transcriptional reprogramming, suggesting that multi-omic coordination may contribute to short-term stress memory.

Overall, our data indicate that the vascular cambium integrates past drought experience through persistent multilayered adjustments, establishing a molecular basis for stress memory that may influence future responses. Future work should integrate temporal and cell-specific omics with hormone localization to clarify functional links between hormonal dynamics and molecular changes.

2. Genetic and epigenetic backgrounds both drive molecular short-term memory

Several features of the short-term memory varied strongly across *P. nigra* genotypes and *P. tremula* × *P. alba* epitypes, demonstrating that both genetic and epigenetic variations modulate drought responses. In *P. nigra*, the genotype originating from Italy (PG-31) displayed higher intrinsic drought tolerance and better growth under water deficit than the genotype from France

(DRA-038). Interestingly, the two genotypes also showed highly divergent response strategies at the molecular level: DRA-038 exhibited stronger hormonal and transcriptional responses, whereas PG-31 showed more limited molecular adjustments but a substantially higher number of DMCs. Increased GA_{12} and cytokinins in DRA-038 suggested resumption of cambial growth, while elevated DPA, an ABA catabolite, pointed to enhanced hormone turnover (W. Ding et al., 2024; Wybouw et al., 2024). However, the downregulation of *UBP13* in DRA-038, a deubiquitinase that stabilizes key components of brassinosteroid signaling (BES1 and BRI1; Park et al., 2022) promoting post-stress growth-related reprogramming (Luo et al., 2022; Xiong et al., 2022) and the upregulation of *SRO1*, a redox-sensitive regulator essential for meristem integrity (Jaspers et al., 2010; Teotia et al., 2009; Teotia & Lamb, 2011), suggested a protective recovery strategy. These observations propound the idea that although growth-promoting hormones were accumulating, the cambium may have prioritized a controlled and protected reactivation of meristem activity over rapid expansion maintaining meristem integrity under the anticipation of recurrent stress. This pattern illustrates a form of the "growth–survival dilemma" described by Claeys & Inzé, 2013, where plants must balance the maintenance of growth and competitiveness against the assurance of survival under water limitation. In our study, DRA-038 tended toward a conservative, survival-oriented strategy characterized by strong hormonal turnover and transcriptional reprogramming, whereas PG-31 maintained growth through epigenetically stabilized pathways, consistent with a resilience-based strategy. Evolutionary history and *in situ* local environments are known to shape epigenomic landscapes across populations and genotypes in tree species including poplar (Vanden Broeck et al., 2024). This likely leads to genotype-specific expressions of stress-induced epigenetic memory.

Contrary to the *P. nigra* genotypes, *P. tremula* × *P. alba* transgenic lines differed only by the targeted modifications of the DNA methylation machinery. Interestingly, these epitypes showed divergent responses to water deficit. Among all epitypes, OX-*dml*, overexpressing a DNA demethylase, showed higher intrinsic drought tolerance and better growth under water deficit. This same epitype also showed altered capacities for symbiotic mycorrhization in previous studies (Vigneaud et al., 2023), reinforcing the general idea that active DNA demethylation does modulate a broad range of important environmentally-responsive traits. OX-*dml* maintained elevated GAs relative to the wild-type and showed a broader transcriptional activation pattern, likely reflecting release from DNA methylation-mediated repression (Xie et al., 2025). Upregulated genes included regulators of water deprivation, auxin transport, and xylem development, consistent with auxin–GA synergy in cambial reactivation (Wybouw et al., 2024). In addition, OX-*dml* also displayed a unique subset of DETs in comparison to the other epitypes, with opposite patterns and often accompanied by differential methylation. For instance, *RAF24* which was constitutively overexpressed and differentially methylated, controls developmental transitions *via* chromatin remodeling (Vanden Broeck et al., 2024; W. Zhou et al., 2025) and is responsive to auxin and osmotic stress (Fàbregas et al., 2020). Its dual regulation at transcriptional and methylation levels makes it a compelling

candidate for the regulation of somatic stress memory, but requires functional validation. Other stress-induced DETs (e.g. *ATS1*, *TAF4*, *ATC3H44*) pointed to coordinated growth-promoting pathways, while repression of *ILLYTHIA* suggested resource allocation away from immune regulation toward growth. Together, these findings emphasize the role of active DNA demethylation in unmasking regulatory networks and enabling epigenetic priming (Zhu et al., 2025), and are consistent with evidence that demethylation participates in xylem development (Lin et al., 2020).

Methylation patterns were highly contrasted between genetic backgrounds. In *P. nigra* genotypes, stress-induced DMCs mostly occurred in CGs within genes, possibly reflecting stable post-stress modifications in contrast to more dynamic CHH methylation already reported in *P. nigra* and other woody species during acute stress (Chen et al., 2012; Sow et al., 2023; Vanden Broeck et al., 2024; Wang et al., 2016). In contrast, in *P. tremula* × *P. alba* epitypes, stress-induced DMCs mainly occurred in CHHs in transposable elements (TEs) (Liang et al., 2014; Sow et al., 2021), while epitype-specific DMCs (relative to the WT), which largely exceeded stress-induced DMCs, were primarily found in CGs within genes. Mechanistically, species differences (*P. nigra* versus *P. tremula* × *P. alba*) in methylation patterns (CG versus CHH) may actually reflect natural variation in the DNA methylation machinery. CHH methylation is established either by the RNA-directed DNA methylation (RdDM) pathway through DRM2, which targets euchromatic sites, or by CMT2, which preferentially methylates long heterochromatic TEs (Stroud et al., 2014, 2014; Xie et al., 2025; Xu & Law, 2024). Stress-induced TE activation is known to be counteracted by RdDM activity, which deposits CHH methylation to repress TE activity and stabilize the genome (Ramakrishnan et al., 2022). This mechanism represents a widespread epigenetic stress response, highlighting the dual role of CHH methylation in immediate protection and potential stress memory. In our study, CHH methylation increased in RNAi-*dml* but decreased in OX-*dml* and RNAi-*ddm1*, suggesting an antagonism between DML activity and the RdDM pathway, possibly mediated by DDM1 (Sow et al., 2021; Xu & Law, 2024). Moreover, a truncated CMT2 allele was identified exclusively in *P. tremula* × *P. alba* (clone INRA 717-1B4) (Fig. S25). Such truncations have previously been linked to genome-wide CHH variability and stress tolerance in Arabidopsis (X. Shen et al., 2014). This hypothesis remains to be functionally validated.

Overlaps between stress-induced DETs, DSEs and DMCs were largely genotype- or epitype-specific. Interestingly, over 70% of genotype- and epitype-specific splicing events co-localized with DMCs in genes associated with chromatin remodeling, pointing to a possible role of methylation in shaping transcript diversity (López Sánchez et al., 2016; Wang et al., 2016), although very few were actually associated with DETs. However, since DNA methylation can act through both cis- and trans-mediated mechanisms (López Sánchez et al., 2016; Wang et al., 2016; Y. Zhang et al., 2020), the lack of overlap between stress-responsive DMCs and DETs or DSE does not preclude any relationships, but may alternatively reflect

trans effects, particularly in epitypes where only methylation was altered. Causality and mechanisms remain to be demonstrated.

Altogether, our data support a model in which somatic memory is dependent upon methylation contexts shaped by genetic predisposition and epitype-specific regulation through multilayered interactions between hormones, transcription (expression and splicing forms), and DNA methylation. Whether this memory enhances stress resilience or plasticity across growing seasons is a key question for perennial species under climate instability.

---

3. Somatic stress memory lasts more than a year and may contribute to priming

Recent models propose that plants retain stress experiences through multilayered imprints involving transcription and epigenetics, forming a persistent molecular memory (Farkas & Dobránszki, 2024). In long-lived perennials, such memory may shape responses across developmental phases and seasons (Gallusci et al., 2023). Our multi-year experiment in *P. nigra* provides empirical support for this hypothesis.

S/C (Stress Year 1 / Control Year 2) trees of the more sensitive genotype DRA-038 showed reduced growth compared to C/C controls in Year 2, suggesting the persistence of a physiological debt, whereas S/C trees of the more tolerant genotype PG-31 were unaffected. In contrast, primed trees subjected to a second water deficit (S/S) showed comparable growth to unprimed trees (C/S) in Year 2, indicating a potential stress-induced acclimation especially in DRA-038. Interestingly, although very different in Year 1, hormonal profiles of primed DRA-038 trees clearly converged toward those of PG-31 in Year 2, with higher auxin and GA and lower cytokinins, possibly favoring xylem differentiation and contributing to partial growth compensation. Differential growth and hormonal patterns were further accompanied by distinct molecular profiles. DETs observed between C/S and S/S trees in Year 2 could be assigned to two distinct categories: type I (sustained from Year 1) and type II (enhanced upon re-exposure to water deficit), which was consistent with the definitions of stress memory in annuals (according to Bäurle & Trindade, 2020). We found six memory DETs in the genotype DRA-038, including reversed expression between Year 1 and Year 2 of *UBP13* and *SRO1*, suggesting a shift from conservative to growth-oriented strategies (see above discussion). Alternatively, we only found two memory DETs in the genotype PG-31, indicating molecular stability rather than flexibility. The limited number of candidates likely reflects the distinction between chromatin-based cis memory and trans memory mediated by transcription factors or hormones (see Farkas & Dobránszki, 2024).

At the methylome level, Year 2 saw a strong increase in CG methylation consistent with their role in stable memory (He & Ecker, 2015; H. Zhang et al., 2018). Most importantly, DRA-038 accumulated *ca.* 20-fold more DMCs than PG-31, converging toward PG-31 Year 1 levels and mirroring hormonal patterns. In addition, the number of DETs colocalizing with DMCs (including *UBP13*) also clearly increased in Year 2, suggesting a possible role for epigenetic regulation of transcriptional long-term memory. Altogether, our data provide

empirical evidence that cambial somatic memory is multilayered (Groover, 2025), genotype-dependent, and can persist over annual timescales (Gallusci et al., 2023). The higher molecular plasticity observed in the intrinsically more sensitive genotype DRA-038 contrasted with the higher stability observed in the intrinsically more tolerant genotype PG-31, and likely reflected distinct adaptive strategies. This supports the concept of epigenetic priming where previous stress history may enhance future responsiveness.

Conclusions

Our study demonstrated that the vascular cambium and cell derivatives may retain molecular imprints of past drought events across growing seasons, establishing somatic memory through coordinated hormonal, transcriptional, and epigenetic remodeling. These signatures mostly represented active reprogramming rather than passive remnants and may support acclimation depending on genotype. In addition, epitype-specific responses demonstrated that DNA methylation alone may contribute to stress memory, likely through combined cis- and trans-mediated effects that influence molecular layers in a cascading manner. Epigenetic memory in the cambium may thus help fine-tuning the balance between growth and survival strategies.

Unlike the transient cambium of *Arabidopsis*, the tree cambium is long-lived and seasonally regulated, integrating environmental cues over years and providing a unique window into long-term molecular and epigenetic memory. Meristematic cells are particularly suited to store stress signatures through hormonal shifts, transcriptional memory, and stable CG methylation marks as shown in the present study (Maury et al., 2019). The maintenance of DNA methylation during cambial cell proliferation is particularly crucial for such stability. Following each mitosis, hemimethylated CpG sites are faithfully restored by MET1, while CHG and CHH methylation depend on the interplay between chromatin context, histone H3K9me2 marks, and siRNA-directed RdDM activity (CMT3 and CMT2 pathways). This division of labor ensures high fidelity for CG methylation but a more variable inheritance of non-CG contexts, leading to differential stability of epigenetic marks within the cambium. Such mechanisms, well described in plant meristems, likely underpin the mitotic memory observed here in a long-lived tissue. Most of our cambial DMC-containing genes (94.5%) could actually be retrieved in other studies reporting methylation-responsive genes in poplar meristems (Fig S26), especially chromatin regulators, reinforcing the functional and evolutionary relevance of these epigenetic changes (Lafon-Placette et al., 2018; Sow et al., 2021, 2023). While histone marks often dominate in annuals, our results indicate that DNA methylation, especially in CG context, provides a robust substrate for long-term stress memory in trees (A.-L. Le Gac et al., 2018; Trontin et al., 2024). Thus, recovery from drought in perennials may involve acclimation through memory-mediated remodeling rather than through a simple return

to baseline (Gessler et al., 2020). Whether this memory enhances resilience or reflects costs of prior stress (Backhaus et al., 2014) remains an open ecological question, but it is central to redefining resilience and plasticity in forest ecosystems facing recurrent drought.

Data availability

The data that support the findings of this study are openly available: The WGBS data have been deposited in the Sequence Read Archive (SRA) at https://www.ncbi.nlm.nih.gov/sra/PRJNA913022/ reference no. PRJNA913022; The RNA-Seq data have been deposited in the SRA at https://www.ncbi.nlm.nih.gov/sra/PRJNA913022/ reference no. PRJNA913022.

The other data described in this Data note can be freely and openly accessed on the Recherche Data Gouv repository under: https://doi.org/10.57745/QZZ2WQ.

Figures

Figure 1. (A) Schematic representation of the experimental design. Experiments were conducted independently on two *P. nigra* (*Pn*) genotypes and four *P. tremula* × *P. alba* (*Ptm* × *Pa*) epitypes. For *Pn* genotypes, experiments were repeated in Year 2 to investigate long-term (transannual) memory of water stress. Abbreviations for treatments: C, control Year 1; S, stressed Year 1; C/C, control Year 1 / control Year 2; C/S, control Year 1 / stressed Year 2; S/S, stressed Year 1 / stressed Year 2; S/C, stressed Year 1 / control Year 2. (B) and (C) Overview of potted trees of *Pn* and *Ptm* × *Pa*, respectively, at the end of the experiment.

Figure 2. Treatment effects on growth and physiological variables in *Populus nigra* (*Pn*) genotypes (A) and *Populus tremula* × *Populus alba* (*Ptm* × *Pa*) epitypes (B) in Year 1. Abbreviations: A_{net}, net CO_2 assimilation; g_s, stomatal conductance to water vapour; $\delta^{13}C_{leaf}$, bulk leaf ^{13}C isotopic composition (more negative values indicate lower intrinsic water-use efficiency); P_{50}, xylem water potential inducing 50% of embolism (more negative values indicate higher intrinsic tolerance to water deficit). P_{50} was estimated only under control conditions. Bars represent mean values ± SE (n = 6 for growth, $\delta^{13}C$ and P_{50} at the end of the experiment; n = 8-9 for A_{net} and g_s spread out throughout the 5-weeks period of water deficit). See Materials and Methods for additional information. Different letters (capital letters for controls, lower case letters for water deficit) indicate significant differences between genotypes within treatments following Tukey's HSD post-hoc test; asterisks indicate significant effects of water deficit (* $0.01 < P \leq 0.05$; ** $0.001 < P \leq 0.01$; *** $P \leq 0.001$).

Figure 3. Effects of the repeated water deficit in Year 2 on growth of the two *Populus nigra* (*Pn*) genotypes. Blue bars are for control (C) trees in Year 2 while red bars are for water-stressed (S) trees; hatched bars are for trees that received a different treatment in Year 1 and Year 2. Abbreviations: C/C, control Year 1 / control Year 2; S/C, stressed Year 1 / control Year 2; C/S, control Year 1 / stressed Year 2; S/S, stressed Year 1 / stressed Year 2. Different letters

indicate significant differences ($P < 0.05$) between treatments following Tukey's HSD post-hoc tests.

Figure 4. Principal component analysis (A-D) and differential analysis (E-F) of the 15 phytohormonal compounds measured by LC-MS in cambium-derived tissues of *Populus nigra* (*Pn*) genotypes (DRA-038 and PG-31) and *Populus tremula* × *P. alba* (*Ptm* × *Pa*) epitypes (WT, OX-*dml*, RNAi-*dml*, RNAi-*ddm1*). A and C) Correlation circles in the two main components for *Pn* genotypes and *Ptm* × *Pa* epitypes, respectively. B and D) Projections of individuals in the main plane for *Pn* genotypes and *Ptm* × *Pa* epitypes for each treatment, respectively. E) Heatmap of hormone variation in response to water deficit for *Pn* genotypes and *Ptm* × *Pa* epitypes. Colours represent the effect size estimate computed as the log2FoldChange (log2FC) of hormone concentrations (in Year 1, red indicates higher concentrations in the water deficit (S) condition relative to the control (C) condition, while blue indicates lower concentrations; in Year 2, red indicates higher concentrations in the S/S treatment relative to the C/S treatment, while blue indicates lower concentrations, grey indicates no data).
Abbreviations: C, control in Year 1; S, stressed in Year 1; C/S, control in Year 1 and stressed in Year 2; S/S, stressed in Years 1 and 2. Auxin (IAA), abscisic acid (ABA), 4'-dihydrophaseic acid (DPA), jasmonic acid (JA), 12-oxo-phytodienoic acid (OPDA), salicylic acid (SA), *cis*-zeatin-O-glucoside cytokinin (cZOG), isopentenyl adenine riboside cytokinin (iPR), *cis*- or *trans*-zeatin riboside cytokinin (cZR or tZR), gibberellin (GA), castasterone (CS), 6-deoxocastasterone (6deoxoCS).

Figure 5. Analysis of differentially expressed transcripts (DETs) in the two *Pn* genotypes (PG-31 and DRA-038) in Year 1 and Year 2. A) Volcano plot and Venn diagram of DETs. Colored dots correspond to DETs that passed the significance threshold (FDR < 0.05) and a log2 fold change threshold of ± 0.5 (blue dots for downregulated, red dots for upregulated); grey dots are for non-DETs. The Venn diagram shows the overlap between the highlighted DETs, the genes in bold are described in Table 2. B) GO enrichment of identified DETs in the two genotypes (PG-31 and DRA-038) in year 2. C) Heatmap of common DETs identified in genotypes for both years. According to the color code of the heatmap, blue corresponds to a decrease and red to an increase of gene expression measured in log2FC. Asterisks (*) in the heatmap represent the genes defined as differentially methylated in the observed conditions. The DETs annotated are presented in Table 2 and Sup_table_2. "Unknown (1)" to "Unknown (4)" correspond respectively to: *Potri.009G005300.9*, *Potri.010G167100.23*, *Potri.013G007900.1* and *Potri.018G114801.1*.

Figure 6. Analysis of differentially expressed transcripts (DETs) in *Ptm* × *Pa* epitypes (WT, OX-*dml*, RNAi-*dml*, RNAi-*ddm1*) in Year 1. A) Volcano plot of DETs between S vs C conditions. Colored dots correspond to DETs that passed the significance threshold (FDR < 0.05) and a log2 fold change threshold of ± 0.5 (blue dots for downregulated, red dots for upregulated DETs); grey dots correspond to non-DETs. The Venn diagram shows the overlap between the highlighted DETs. B) GO enrichment of DETs in WT and OX-*dml* epitypes in year 1 (OX-*dml* was chosen as the most resistant to water deficit based on ecophysiological data, Fig. 2). Metascape analyses for RNAi-*dml* and RNAi-*ddm1* are available in Fig_S10).

C) Heatmap of the stress-induced 46 DETs (S *versus* C) identified in at least two of the four epitypes. The annotation of these genes is available in Sup_table_3. According to the color code of the heatmap, blue corresponds to a decrease and red to an increase in gene expression measured as the log2FC. D) Heatmaps of the epitype-DETs (line vs. WT) showing opposite expression in C or S conditions and the annotation of candidate genes are described in Sup_table_4. Asterisks (*) in the heatmaps represent the genes observed as differentially methylated.

Figure 7. Number of Differentially Methylated Cytosines (DMCs) per methylation context (CG, CHG, CHH). A) DMCs in *Pn* genotypes (DRA-038 and PG-31) in response to treatments in Year 1 (S *vs*. C) and Year 2 (S/S *vs*. C/S). B) DMCs between control greenhouse conditions (this study) and previously published data from an outdoor common garden in the two *Pn* genotypes (DRA-038 and PG-31) and DMCs between genotypes located in the greenhouse (this study) or outdoor common garden (Sow et al. 2023). DMCs in the common garden were obtained from three years old clonal copies of the same genotypes installed in an outdoor common garden (details on the experimental setup are available in Sow et al. 2023). C) DMCs in *Ptm* × *Pa* epitypes (WT, OX-*dml*, RNAi-*dml*, RNAi-*ddm1*) in response to treatment in Year 1 (S *vs*. C). D) DMCs between *Ptm* × *Pa* WT and other epitypes (OX-*dml*, RNAi-*dml* or RNAi-*ddm1*) under control (C) or stressed (S) conditions.

Figure 8. Characterization of differentially methylated cytosines (DMCs) identified in *Pn* genotypes and *Ptm* × *Pa* epitypes. A) General distribution of stress-induced DMCs between features in *Pn* genotypes (DRA-038 and PG-31) and *Ptm* × *Pa* epitypes (WT, OX-*dml*, RNAi-*dml*, RNAi-*ddm1*) in Year 1 (S *vs*. C), and genes containing DMCs were subsequently annotated (Sup_table_6). B) Number of stress-induced DMCs in transposable elements in *Pn* genotypes in Year 1 (S *vs*. C) and Year 2 (S/S *vs*. C/S). C) Number of stress-induced DETs in *Pn* genotypes classified as either "ON/OFF" (transcripts detected exclusively in one condition, absent in the other) or "Quantitative" (transcripts detected in both conditions with significant differential expression, $\log_2 FC > 0.5$, $p < 0.05$). DETs were further categorized according to the methylation status of their associated gene (DMCs vs. no DMC). D) Number of stress-induced DMCs in transposable elements in *Ptm* × *Pa* epitypes in Year 1 (S *vs*. C). E) Number of stress-induced DETs (ON/OFF vs. quantitative) showing either no DMC or DMCs within the genes in *Ptm* × *Pa* epitypes. F) Number of *Ptm* × *Pa* line-specific DMCs (comparison relative to WT) in transposable elements in Year 1. G) Number of line-specific DETs (ON/OFF vs. quantitative) showing either no DMC or DMCs within the genes under control (C) or stressed (S) conditions in Year 1 in *Ptm* × *Pa* epitypes. Gene-level annotations are provided in the table (sup_table_7).

Table

Table 1. Denomination and characteristics of the plant material used in the study

Table 2. Overview of the candidate genes found in the differential expression (DET) or differential splicing (DSE) analyses carried out by genotype in *Pn* (Fig 5A; see also Sup_table_2. For more details).

Supporting information

Sup _table_1. Summary table of the main trends observed on the measurement of the 15 analyzed phytohormones in the cambium : IAA (Auxine), ABA (Abscisic Acid), DPA (4'-dihydrophaseic acid; ABA derivative), JA (Jasmonic acid), OPDA (oxylipin 12-oxo-phytodienoic acid, JA derivative), SA (Salicylic Acid), cZOG (cis-Zeatin-O-glucoside; Cytokinin), iPR (Isopentenyl adenine riboside; Cytokinin), tZR (Trans-zeatin riboside; Cytokinin), cZR (cis-Zeatin riboside; Cytokinin), GA8, GA12, GA19 (Gibberellins), CS (castasterone; Brassinosteroid), 6-deoxoCS (6-Deoxocastasterone; Brassinosteroid)

Sup_Table_2. List of genes of interest identified through various analyses (differential expression, differential splicing event) for *Pn* genotypes. Each gene is annotated to its putative Arabidopsis thaliana orthologue, functional annotation and literature references.

Sup_Table_3. Annotation of the list of 46 DETs identified in at least two of the four epitypes in the heatmap of Fig. 6. Each gene is annotated to its putative Arabidopsis thaliana orthologue, functional annotation and literature references.

Sup_Table_4. List of genes of interest identified through various analyses (differential expression, alternative splicing) for *Ptm* × *Pa* epitypes. Each gene is annotated to its putative Arabidopsis thaliana orthologue, functional annotation and literature references.

Sup_Table_5. List of DETs with memory-related and/or epitype-specific DSE classification in the *Ptm* × *Pa* epitypes comparison. The table includes 12 memory-related and 30 epitype-specific genes also classified as DETs. Each gene is annotated to its putative Arabidopsis thaliana orthologue, functional annotation and literature references.

Sup_Table_6. Annotated genes containing stress-induced DMCs in *Pn* genotypes (DRA-038 and PG-31) and *Ptm* × *Pa* epitypes (WT, OX-dml, RNAi-dml, RNAi-ddm1) in Year 1 (S vs. C)."

Sup_Table_7. List of differentially expressed transcripts (DETs) detected in *Pn* genotypes and *Ptm* × *Pa* epitypes. For each gene, an astérisque in “DET_ON/OFF” or “DET_Quantitative” denotes the expression category (ON/OFF vs. quantitative), and an astérisque in “DET_with_DMC” or “no_DMC” denotes the presence or absence of a cis-DMC, respectively.

Fig_S1. Time course of soil relative extractable water (REW), height and diameter growth during the experiment in *Populus nigra* (*Pn*) genotypes and *Populus tremula* × *P. alba* (*Ptm* × *Pa*) epitypes. t_0 corresponds to the onset of the five-weeks water deficit; the dashed lines indicate the day of rewatering. Values correspond to means ± SE (n = 6).

Fig_S2. Histological characterization (light microscopy) of the cambial sampling strategy for genomic and phytohormone analyses. (A) Non-split, non-scratched stem showing secondary xylem and phloem tissues originating from the vascular cambium. The active central cambial zone already appears brittle. (B) Portion of the bark side after splitting but before scratching. The arrows indicate that after splitting most, but not all, of the cambial cells remained on this side. (C) Portion of the bark side after scratching. The asterisks highlight the most apparent areas corresponding to the sampled tissue fraction on the bark side. (D) Portion of the stem side after scratching. The asterisks highlight the most apparent areas corresponding to the sampled tissue fraction on the stem side. **cp**, cortical parenchyma; **cz**, cambial

zone; **mp**, mature secondary phloem; **mx**, mature secondary xylem; **pf**, secondary phloem fibers; **yp**, young differentiating secondary phloem; **yx**, young differentiating secondary xylem.
Semi-thin (1µm) stem cross-sections were obtained with an ultracut R microtome (Leica, Rueil-Malmaison, France) from larger sections embedded in medium-grade LR White resin and were stained with toluidine blue O 0.1% (w/v) (Sigma-Aldrich). Stained sections were then examined under a light microscope (Leica DMR) coupled with a Leica DFC 320 digital camera (100× magnification).

Fig_S3. Principal Component Analysis (PCA) of 15 phytohormone concentrations measured in cambium-derived tissues from two Populus nigra natural genotypes (DRA-038 and PG-31) grown under control (C) and recurrent drought (S) treatments. (A) shows the projection of samples along principal components 1 and 3 (PC1 × PC3), highlighting treatment effects and genotype-specific clustering. (B) displays the correlation circle for the same components, where arrows indicate the contribution and orientation of each hormone variable to the PCA axes. (C) summarizes the percentage of total variance explained by the first principal components, illustrating the relative contribution of PC1–PC5 to overall variability.

Fig_S4. Principal Component Analysis (PCA) of 15 phytohormone concentrations measured in cambium-derived tissues from *Ptm* × *Pa* epitypes (RNAi-*dml*, OX-*dml*, RNAi-*ddm1*, and WT) subjected to control and drought conditions. (A) represents the distribution of samples along PC1 and PC3, emphasizing differences among epitypes and treatments. (B) shows the correlation circle (PC1 × PC3), illustrating the relative contribution of each hormone to the ordination space. (C) displays the proportion of variance explained by the first five principal components, indicating the main axes of variability in hormonal profiles.

Fig_S5. Heatmap of hormone variation in control or stress condition during the treatment for *Pn* genotypes (DRA-038 versus PG-31) and *Ptm* × *Pa* epitypes (versus WT). Colours represent the effect size estimate computed as the log2FoldChange (log2FC) of hormone concentrations (red indicates higher concentrations, while blue indicates lower concentrations).

Fig_S6. Venn diagram representing the number of detected transcripts, and DETs in brackets. (A) Transcripts and DET detected after stress conditions (drought-rewatered) for *Pn* genotypes and *Ptm* × *Pa* epitypes. (B-C) Transcripts and DET are different for each *Ptm* × *Pa* epitypes versus the wild-type in (B) control conditions and (C) stress conditions.

Fig_S7. Number and overlap of DETs between *Pn* genotypes (DRA-038, PG-31) under control and water stress conditions across two years. Bar plots show the total number of DETs identified between DRA-038 and PG-31 under control and stress conditions in Year 1 (Y1) and Year 2 (Y2). Venn diagrams display the overlap of DETs across years under control and stress conditions. Numbers represent DETs unique to each year or shared between years.

Fig_S8. Overlap of differentially expressed transcripts (DETs) among *Pn* genotypes and *Ptm* × *Pa* epitypes under control and stress conditions. (A) Venn diagram showing shared and unique DETs between natural genotypes DRA-038 and PG-31 across two consecutive years. (B) Venn diagram showing shared DETs among *Ptm* × *Pa* epitypes (RNAi-ddm1, RNAi-dml, and OX-dml) and wild type (WT) in Year 1. (C–D) Venn diagrams showing the overlap of DETs among *Ptm* × *Pa* epitypes under control (C) and drought stress (D) conditions. Numbers indicate the count of DETs specific to or shared between groups.

Fig_S9. Distribution and functional enrichment of Differential Splicing Events (DSEs) detected in *Pn* genotypes and *Ptm* × *Pa* epitypes. (A) Pie charts showing the relative proportion of DSE types identified in *P. nigra* genotypes (PG-31 and DRA-038) across two consecutive years, and in *Ptm* × *Pa* epitypes (*RNAi-ddm1*, *RNAi-dml*, and *OX-dml*) under control (C) and drought stress (S) conditions. Event types include skipped exon (SE), alternative 5′ splice site (A5SS), alternative 3′ splice site (A3SS), retained intron (RI), mutually exclusive exons (MX), alternative first exon (AF), and alternative last exon (AL). (B) Gene Ontology (GO) enrichment analysis of genes carrying DSEs overlapping with Differentially Methylated Genes (DMGs).

Fig_S10. DETs and enriched GO terms in *Ptm* × *Pa* epitypes during Year 1 treatment. (A) Venn diagram showing the overlap of DETs (adjusted p-value < 0.05) identified in *Ptm* × *Pa* epitypes (WT, RNAi-*ddm1*, RNAi-*dml*, OX-*dml*) under control conditions during Year 1 treatment. (B) Bar plots displaying the top significantly enriched GO term associated with DETs in each epitype.

Fig_S11. Differential gene expression in *Ptm* × *Pa* epitypes under control and stress conditions. (A–B) Volcano plots showing differentially expressed transcripts (DETs) in each epitype (RNAi-*ddm1*, RNAi-*dml*, and OX-*dml*) compared to the wild type (WT) under control (A) and drought stress (B) conditions. The x-axis represents the $\log_2$ fold change ($\log_2$FC), and the y-axis represents the statistical significance ($-\log_{10}$ p-value). Red dots indicate up-regulated genes, blue dots indicate down-regulated genes, and gray dots represent non-significant changes. (C) Venn diagram showing the overlap of DETs among *Ptm* × *Pa* epitypes under control (C) and stress (S) conditions. Numbers indicate the count of transcripts that are condition- or epitype-specific, or shared across multiple conditions or genotypes.

Fig_S12. Heatmap of DETs across *Pn* genotypes and *Ptm* × *Pa* epitypes in response to Year 1 treatment. The heatmap shows the $\log_2$FC in expression levels of DETs across *Pn* genotypes (DRA-038, PG-31) and *Ptm* × *Pa* epitypes (WT, RNAi-*ddm1*, OX-*dml* and RNAi-*dml*). Gene expression is color-coded from blue (down-regulated) to red (up-regulated). Gray boxes indicate missing or non-significant data. Gene identifiers from Arabidopsis thaliana and Populus trichocarpa are provided alongside predicted gene functions. Asterisks (*) mark genes with statistically significant differentially methylated.

Fig_S13. DETs and enriched GO terms in *Ptm* × *Pa* epitypes under control conditions (well-watered). (A) Venn diagram showing the overlap of DETs (adjusted p-value < 0.05) among the *Ptm* × *Pa* epitypes RNAi-*ddm1*, RNAi-*dml*, and OX-*dml* under C conditions. (B) Bar plots displaying the top significantly enriched GO biological processes associated with DETs in each epitype.

Fig_S14. DETs and enriched GO terms in *Ptm* × *Pa* epitypes under S conditions (WD-RW). (A) Venn diagram showing the overlap of DETs (adjusted p-value < 0.05) among the *Ptm* × *Pa* epitypes RNAi-*ddm1*, RNAi-*dml*, and OX-*dml* under S conditions. (B) Bar plots displaying the top significantly enriched GO term associated with DETs in each epitype.

Fig_S15. Conservation of DMCs in *Pn* genotypes across methylation contexts and environmental conditions. Bar plot showing the percentage of conserved DMCs in three methylation contexts (CG, CHG, CHH) across different comparisons involving genotypes (DRA-038 and PG-31), environmental conditions (greenhouse vs. garden), treatments (control, stress), and memory effects. Categories include DMCs conserved among environments, across plastic responses, memory, and between genotypes.

Fig_S16. DMCs in transposable elements (TEs) across genotypes, epitypes, and conditions. (A–D) Bar plots (left) show the number of hypermethylated (red) and hypomethylated (blue) differentially methylated cytosines (DMCs) in TEs; Venn diagrams (right) show the overlap of differentially

methylated TEs (DMTEs). (A) *Pn* genotypes PG-31 and DRA-038 across Year 1 and Year 2. (B) *Ptm* × *Pa* epitypes (WT, RNAi-*ddm1*, RNAi-*dml*, OX-*dml*) under Year 1 treatment. (C) Epitypes under C conditions. (D) Epitypes under S conditions.

Fig_S17. Distribution of differentially methylated transposable elements (DMTEs) by TE class. Pie chart showing the proportion of DMTEs across transposable element (TE) classes in the full dataset (P1), the *Pn* genotypes dataset (P2), the *Ptm* × *Pa* epitypes (Year 1) dataset (P3), the *Ptm* × *Pa* epitypes C conditions dataset (P4), the *Ptm* × *Pa* epitypes S conditions dataset (P5).

Fig_S18. Overlap of differentially methylated genes (DMG) across *Pn* genotypes and *Ptm* × *Pa* epitypes and conditions. (A) Venn diagram showing the overlap of DMG in *Pn* genotypes (DRA-038, PG-31) across two years treatment (Year 1 and Year 2). (B) Venn diagram showing the overlap of DMG among *Ptm* × *Pa* epitypes (WT, RNAi-*ddm1*, RNAi-*dml*, OX-*dml*) during Year 1 treatment. (C) Venn diagram showing DMG shared or unique among epitypes under C control conditions. (D) Venn diagram showing DMCs shared or unique among epitypes under S conditions.

Fig_S19. GO term enrichment of DMG in *Pn* genotypes (DRA-038, PG-31) across both years treatment (Year 1 and Year 2 only for DRA-038). Bar plots showing the top significantly enriched GO term associated with genes overlapping differentially methylated regions in *Pn* genotypes during Year 1 and Year 2. The bottom right panel shows GO terms commonly enriched in both years.

Fig_S20. Proportion of transposable element (TE) classes among differentially methylated TEs (DMTEs) detected in *Pn* genotypes and *Ptm* × *Pa* epitypes. Pie charts show the relative distribution of TE superfamilies among DMTEs identified for each comparison and condition (e.g., between genotypes, years, or treatments). TE classes were annotated according to the *P. trichocarpa* v4.1 genome annotation.

Fig_S21. Bar plots showing the top significantly enriched GO term for DMG in *Ptm* × *Pa* epitypes (WT, RNAi-*ddm1*, RNAi-*dml*, OX-*dml*).

Fig_S22. Bar plots showing enriched GO term for genes both differentially expressed and differentially methylated (DET–DMG) in the OX-*dml* epitype. Qualitative analysis (ON/OFF) identifies GO terms associated with gene activation or silencing events. Quantitative analysis highlights GO terms based on magnitude of expression changes.

Fig_S23. Pie charts show the proportion of DSE types among all DSEs genes (left), only DSE genes overlapping with DMG (center), and DSEs without DMG overlapping (right). Event types include skipped exon (SE), alternative 5′ splice site (A5SS), alternative 3′ splice site (A3SS), retained intron (RI), mutually exclusive exons (MX), alternative first exon (AF), and alternative last exon (AL).

Fig_S24. Proportion of DMG in DSE genes in *Ptm* × *Pa* epitypes and *Pn* genotypes. (A) Bar plot showing the number of DSE genes, including those overlapping DMG, across genotypes, epitypes, years (Y1, Y2), and conditions (C: control; S: stress). (B) GO term enrichment of genes showing constitutive DSE and DMG. (C) Gene model of *Potri.019G052500*, showing the distribution of the 314 DMCs, with hypermethylated (red) and hypomethylated (blue) DMCs across the gene body in RNAi-*ddm1* in S condition. Pie chart summarizes genomic features associated with the DMCs, with a focus on the skipped exon (indicated by arrow).

Fig_S25. Sequence alignment and conservation analysis of PtaDML6 homologs. Multiple sequence alignment of PtaDML6 with homologous proteins, displaying residue-level conservation scores, consensus sequences, and quality metrics across aligned regions. Bar plots indicate conservation (yellow) and alignment quality (brown), with black bars marking the disorder probability. Alignment was performed using the Jalview platform.

Fig_S26. Proportion of genes showing overlap between differential expression and methylation across published studies. Bar plot showing the percentage of genes identified as both differentially methylated (DMG) and differentially expressed (DEG) in poplar species, tissues, and environmental contexts, based on published datasets. Studies include shoot apical meristem (SAM) and cambium under conditions such as control (Well-watered), cold, water deficit, rewatering, and contrasting field environments. 1 = Lafon Placette et al. 2013, *P. tm* × *P. a* (INRA clone 717 1B4), SAM, control, euchromatin methylated genes. 2 = Lafon Placette et al. 2018, *P. deltoides* × *Pn*, SAM, control/water deficit/water deficit-rewatering, DEG/DMG. 3 = Condé et al. 2017, *P. tm* × *P. a* (INRA clone 717 1B4), SAM, control/cold, DEG/DMG. 4 = Le Gac et al. 2018, *P. deltoides* × *Pn*, SAM, three pedoclimatic sites, DEG/DMG. 5 = Sow et al. 2021, *P. tm* × *P. a* (INRA clone 717 1B4), SAM, control/water deficit-rewatering, DEG/DMG. 6 = Sow et al. 2023, *Pn*, cambium, natural common garden, expression level. 7 = Kim et al. 2019, *P. alba* × *P. glandulosa*, cambium (three developmental stages), control, DEG. 8 = Orthologous gene epigenetic modifier for poplar.

Author Contributions

S.M. and R.F. coordinated the research. The plant experimental design was established by V.S., I.A., S.S., R.F. and S.M. Plant growth and phenotypic assessments were performed by G.L., A.D., I.L.J., P.P under the supervision of R.F. Hormones analyses by LC-MS were done by Y-Q.F and B-D.C. Hydraulic analyses were done by R.F., G.L., I.L.J. and H.C. Histochemical and microscopic analysis were done by F.L. and R.F. Molecular analyses were performed by A.D., M.D.S. Statistics were performed by A.D. and R.F. Methylome sequencing was performed by J.T. and C.D. Bioinformatic analyses were done by A.D., A.T., O.R., and S.M.. The draft manuscript was conceived and written by A.D., R.F. and S.M., and further revised by H.D., V.J., L.S., J.T., V.S. All authors approved the final version of the article. We would like to pay a warm tribute to our co-author and friend Alain Delaunay, who passed away in August 2024. He joined the P2e lab (formerly LBLGC) of the University of Orléans (FRANCE) in 2000 and did outstanding work on epigenetic analysis in trees for several (inter)national projects and publications.

Acknowledgements

This work benefited from the equipment and services coordinated by Y. Marie for the RNA-seq analyses conducted at the IGenSeq platform (ICM, Paris, France). Scientific and technical support was provided by the Epigenomic Environmental Platform of IHPE (http://ihpe.univperp.fr/plateforme-epigenetique/; Cristian Chapparo, Perpignan, France). We thank the GENOTOUL platform for providing computational storage space. Isotopic and elemental analyses were performed by the SILVATECH platform (Silvatech, INRAE, 2018; Structural and Functional Analysis of Tree and Wood Facility, DOI: 10.15454/1.5572400113627854E12), involving UMR 1434 SILVA, 1136 IAM, 1138 BEF, and EA 4370 LERMAB at the INRAE Grand-Est Nancy research center. The SILVATECH facility is supported by the French National Research Agency (ANR) through the Laboratory of Excellence ARBRE (ANR-11-LABX-0002-01). We would also like to thank the Tree Cell Engineering Laboratory (LICA) (https://www6.inrae.fr/in-sylva-france_eng/Services/In-Lab/LICA), where the GM plants were grown and characterized. Finally, we are grateful to the GBFOR facility (INRAE, 2018; Forest Genetics and Biomass Facility, DOI: 10.15454/1.5572308287502317E12) for its contribution to the experimental design setup and sample collection. We also acknowledge the GDR 3E network (Epigenetics in Ecology and Evolution, coordinated by Christoph Grunau) for stimulating scientific exchanges, and the members and coordinators (including S.M.) of the COST Actions Epigenetic mechanisms of Crop Adaptation To Climate cHange (EPICATCH, CA19125) and Innovative Woody Plant Cloning (COPYTREE, CA21157) for their constructive discussions. We thank Professor Steven H. Strauss and his team (Department of Forest Ecosystems and Society, Oregon State University, Corvallis, Oregon, USA) for providing the poplar RNAi-ddm1 lines. We are grateful to Julien Vigneaud for valuable discussions related to the EPITREE project, and to Vanina Benoit and Corinne Buret (UMR BioForA, Orléans) for their assistance with sample collection.

Funding

A.D. and M.D.S. received PhD grants from the Conseil Régional du Centre-Val de Loire (France) or the French Ministry of Higher Education and Research (MESR), respectively. This work was supported by the Agence Nationale pour la Recherche (ANR, France) through the EPITREE project (grant no. ANR-17-CE32-0009, Coord. S.M.).

Conflict of interest statement. None declared.

References

Akalin, A., Kormaksson, M., Li, S., Garrett-Bakelman, F. E., Figueroa, M. E., Melnick, A., & Mason, C. E. (2012). methylKit : A comprehensive R package for the analysis of genome-wide DNA methylation profiles. *Genome Biology*, *13*(10), R87. https://doi.org/10.1186/gb-2012-13-10-r87

Alves, M. S., Fontes, E. P. B., & Fietto, L. G. (2011). EARLY RESPONSIVE to DEHYDRATION 15, a new transcription factor that integrates stress signaling

pathways. *Plant Signaling & Behavior*, *6*(12), 1993-1996. https://doi.org/10.4161/psb.6.12.18268

Amaral, J., Ribeyre, Z., Vigneaud, J., Sow, M. D., Fichot, R., Messier, C., Pinto, G., Nolet, P., & Maury, S. (2020). Advances and Promises of Epigenetics for Forest Trees. *Forests*, *11*(9), Article 9. https://doi.org/10.3390/f11090976

Backhaus, S., Kreyling, J., Grant, K., Beierkuhnlein, C., Walter, J., & Jentsch, A. (2014). Recurrent Mild Drought Events Increase Resistance Toward Extreme Drought Stress. *Ecosystems*, *17*(6), 1068-1081. https://doi.org/10.1007/s10021-014-9781-5

Bäurle, I., & Trindade, I. (2020). Chromatin regulation of somatic abiotic stress memory. *Journal of Experimental Botany*, *71*(17), 5269-5279. https://doi.org/10.1093/jxb/eraa098

Bouyer, L., Vincent-Barbaroux, C., Le Jan, I., Delaunay, A., Marchand, L., Feinard-Duranceau, M., Sallé, A., Chassagnaud, D., Barigah, T. S., Cochard, H., Brignolas, F., & Fichot, R. (2023). Concurrent time course of xylem hydraulic dysfunction and non-structural carbohydrates under contrasting water deficits and nitrogen supplies in poplar. *Environmental and Experimental Botany*, *206*, 105173. https://doi.org/10.1016/j.envexpbot.2022.105173

Brenya, E., Pervin, M., Chen, Z.-H., Tissue, D. T., Johnson, S., Braam, J., & Cazzonelli, C. I. (2022). Mechanical stress acclimation in plants : Linking hormones and somatic memory to thigmomorphogenesis. *Plant, Cell & Environment*, *45*(4), 989-1010. https://doi.org/10.1111/pce.14252

Cai, B.-D., Yin, J., Hao, Y.-H., Li, Y.-N., Yuan, B.-F., & Feng, Y.-Q. (2015). Profiling of phytohormones in rice under elevated cadmium concentration levels by magnetic solid-phase extraction coupled with liquid chromatography tandem mass spectrometry. *Journal of Chromatography A*, *1406*, 78-86. https://doi.org/10.1016/j.chroma.2015.06.046

Chateigner, A., Lesage-Descauses, M.-C., Rogier, O., Jorge, V., Leplé, J.-C., Brunaud, V., Roux, C. P.-L., Soubigou-Taconnat, L., Martin-Magniette, M.-L., Sanchez, L., & Segura, V. (2020). Gene expression predictions and networks in natural populations supports the omnigenic theory. *BMC Genomics*, *21*(1), 416. https://doi.org/10.1186/s12864-020-06809-2

Chen, M.-L., Fu, X.-M., Liu, J.-Q., Ye, T.-T., Hou, S.-Y., Huang, Y.-Q., Yuan, B.-F., Wu, Y., & Feng, Y.-Q. (2012). Highly sensitive and quantitative profiling of acidic phytohormones using derivatization approach coupled with nano-LC–ESI-Q-TOF-MS analysis. *Journal of Chromatography B*, *905*, 67-74. https://doi.org/10.1016/j.jchromb.2012.08.005

Claeys, H., & Inzé, D. (2013). The Agony of Choice : How Plants Balance Growth and Survival under Water-Limiting Conditions. *Plant Physiology*, *162*(4), 1768-1779. https://doi.org/10.1104/pp.113.220921

Cochard, H., Damour, G., Bodet, C., Tharwat, I., Poirier, M., & Améglio, T. (2005). Evaluation of a new centrifuge technique for rapid generation of xylem vulnerability curves. *Physiologia Plantarum*, *124*(4), 410-418. https://doi.org/10.1111/j.1399-3054.2005.00526.x

Cohen, D., Bogeat-Triboulot, M.-B., Tisserant, E., Balzergue, S., Martin-Magniette, M.-L., Lelandais, G., Ningre, N., Renou, J.-P., Tamby, J.-P., Le Thiec, D., & Hummel, I. (2010). Comparative transcriptomics of drought responses in Populus : A meta-analysis of genome-wide expression profiling in mature leaves and root apices across two genotypes. *BMC Genomics*, *11*, 630. https://doi.org/10.1186/1471-2164-11-630

Conde, D. (2017a). Chilling-responsive DEMETER-LIKE DNA demethylase mediates in poplar bud break. *Plant, Cell & Environment*, *40*(10), 2236-2249. https://doi.org/10.1111/pce.13019

Conde, D. (2017b). Overexpression of DEMETER, a DNA demethylase, promotes early apical bud maturation in poplar. *Plant, Cell & Environment*, *40*(11), 2806-2819. https://doi.org/10.1111/pce.13056

Conde, D., Le Gac, A.-L., Perales, M., Dervinis, C., Kirst, M., Maury, S., González-Melendi, P., & Allona, I. (2017). Chilling-responsive DEMETER-LIKE DNA demethylase mediates in poplar bud break. *Plant, Cell & Environment*, *40*(10), 2236-2249. https://doi.org/10.1111/pce.13019

Crisp, P. A., Ganguly, D., Eichten, S. R., Borevitz, J. O., & Pogson, B. J. (2016). Reconsidering plant memory : Intersections between stress recovery, RNA turnover, and epigenetics. *Science Advances*, *2*(2), e1501340. https://doi.org/10.1126/sciadv.1501340

Ding, J., Mao, L.-J., Wang, S.-T., Yuan, B.-F., & Feng, Y.-Q. (2013). Determination of Endogenous Brassinosteroids in Plant Tissues Using Solid-phase Extraction with Double Layered Cartridge Followed by High-performance Liquid Chromatography–Tandem Mass Spectrometry. *Phytochemical Analysis*, *24*(4), 386-394. https://doi.org/10.1002/pca.2421

Ding, W., Wang, C., Mei, M., Li, X., Zhang, Y., Lin, H., Li, Y., Ma, Z., Han, J., Song, X., Wu, M., Zheng, C., Lin, J., & Zhao, Y. (2024). Phytohormones involved in vascular cambium activity in woods : Current progress and future challenges. *Frontiers in Plant Science*, *15*. https://doi.org/10.3389/fpls.2024.1508242

Dobin, A., Davis, C. A., Schlesinger, F., Drenkow, J., Zaleski, C., Jha, S., Batut, P., Chaisson, M., & Gingeras, T. R. (2013). STAR : Ultrafast universal RNA-seq aligner. *Bioinformatics (Oxford, England)*, *29*(1), 15-21. https://doi.org/10.1093/bioinformatics/bts635

Dowen, R. H., Pelizzola, M., Schmitz, R. J., Lister, R., Dowen, J. M., Nery, J. R., Dixon, J. E., & Ecker, J. R. (2012). Widespread dynamic DNA methylation in response to biotic stress. *Proceedings of the National Academy of Sciences*, *109*(32), E2183-E2191. https://doi.org/10.1073/pnas.1209329109

Doyle, J. J., & Doyle, J. L. (Éds.). (1987). A rapid DNA isolation procedure for small quantities of fresh leaf tissue. *PHYTOCHEMICAL BULLETIN*.

Dugé de Bernonville, T., Daviaud, C., Chaparro, C., Tost, J., & Maury, S. (2022). From Methylome to Integrative Analysis of Tissue Specificity. In V. Courdavault & S. Besseau (Éds.), *Catharanthus roseus : Methods and Protocols* (p. 223-240). Springer US. https://doi.org/10.1007/978-1-0716-2349-7_16

Duursma, R., & Choat, B. (2017). fitplc—An R package to fit hydraulic vulnerability curves. *Journal of Plant Hydraulics*, *4*, e002-e002. https://doi.org/10.20870/jph.2017.e002

Fàbregas, N., Yoshida, T., & Fernie, A. R. (2020). Role of Raf-like kinases in SnRK2 activation and osmotic stress response in plants. *Nature Communications*, *11*(1), 6184. https://doi.org/10.1038/s41467-020-19977-2

Faivre-Rampant, P. P., Zaina, G., Jorge, V. V., Giacomello, S., Segura, V., Scalabrin, S., Guérin, V., Paoli, E. de, Aluome, C., Viger, M., Cattonaro, F., Payne, A., Paulstephenraj, P. S., Paslier, M.-C. L., Berard, A. A., Allwright, M., Villar, M. M., Taylor, G., Bastien, C., & Morgante, M. (2016). New resources for genetic studies in Populus nigra : Genome-wide SNP discovery and development of a 12k Infinium array. *Molecular Ecology Resources*, *16*(4), 1023. https://doi.org/10.1111/1755-0998.12513

Farkas, D., & Dobránszki, J. (2024). Vegetal memory through the lens of transcriptomic changes—Recent progress and future practical prospects for exploiting plant transcriptional memory. *Plant Signaling & Behavior*, *19*(1), 2383515. https://doi.org/10.1080/15592324.2024.2383515

Fichot, R., Brignolas, F., Cochard, H., & Ceulemans, R. (2015). Vulnerability to drought-induced cavitation in poplars : Synthesis and future opportunities. *Plant, Cell & Environment*, *38*(7), 1233-1251. https://doi.org/10.1111/pce.12491

Fukuda, H. (2004). Signals that control plant vascular cell differentiation. *Nature Reviews Molecular Cell Biology*, *5*(5), 379-391. https://doi.org/10.1038/nrm1364

Gallusci, P., Agius, D. R., Moschou, P. N., Dobránszki, J., Kaiserli, E., & Martinelli, F. (2023). Deep inside the epigenetic memories of stressed plants. *Trends in Plant Science*, *28*(2), 142-153. https://doi.org/10.1016/j.tplants.2022.09.004

Galviz, Y. C. F., Ribeiro, R. V., & Souza, G. M. (2020). Yes, plants do have memory. *Theoretical and Experimental Plant Physiology*, *32*(3), 195-202. https://doi.org/10.1007/s40626-020-00181-y

Gebreselassie, M. N., Ader, K., Boizot, N., Millier, F., Charpentier, J.-P., Alves, A., Simões, R., Rodrigues, J. C., Bodineau, G., Fabbrini, F., Sabatti, M., Bastien, C., & Segura, V. (2017). Near-infrared spectroscopy enables the genetic analysis of chemical properties in a large set of wood samples from Populus nigra (L.) natural populations. *Industrial Crops and Products*, *107*, 159-171. https://doi.org/10.1016/j.indcrop.2017.05.013

Gessler, A., Bottero, A., Marshall, J., & Arend, M. (2020). The way back : Recovery of trees from drought and its implication for acclimation. *New Phytologist*, *228*(6), 1704-1709. https://doi.org/10.1111/nph.16703

Groover, A. (2025). Roles for epigenetics in wood formation and stress response intrees–from basic biology to forest management. *Frontiers in Epigenetics and Epigenomics*, *3*. https://doi.org/10.3389/freae.2025.1476499

Guet, J., Fabbrini, F., Fichot, R., Sabatti, M., Bastien, C., & Brignolas, F. (2015). Genetic variation for leaf morphology, leaf structure and leaf carbon isotope discrimination in European populations of black poplar (Populus nigra L.). *Tree Physiology*, *35*(8), 850-863. https://doi.org/10.1093/treephys/tpv056

Hammond, W. M., Williams, A. P., Abatzoglou, J. T., Adams, H. D., Klein, T., López, R., Sáenz-Romero, C., Hartmann, H., Breshears, D. D., & Allen, C. D. (2022). Global field observations of tree die-off reveal hotter-drought fingerprint for Earth's forests. *Nature Communications*, *13*(1), 1761. https://doi.org/10.1038/s41467-022-29289-2

Harris, C. J., Amtmann, A., & Ton, J. (2023). Epigenetic processes in plant stress priming : Open questions and new approaches. *Current Opinion in Plant Biology*, *75*, 102432. https://doi.org/10.1016/j.pbi.2023.102432

He, Y., & Ecker, J. R. (2015). Non-CG Methylation in the Human Genome. *Annual review of genomics and human genetics*, *16*, 55-77. https://doi.org/10.1146/annurev-genom-090413-025437

Hilker, M., Schwachtje, J., Baier, M., Balazadeh, S., Bäurle, I., Geiselhardt, S., Hincha, D. K., Kunze, R., Mueller-Roeber, B., Rillig, M. C., Rolff, J., Romeis, T., Schmülling, T., Steppuhn, A., van Dongen, J., Whitcomb, S. J., Wurst, S., Zuther, E., & Kopka, J. (2016). Priming and memory of stress responses in organisms lacking a nervous system. *Biological Reviews of the Cambridge Philosophical Society*, *91*(4), 1118-1133. https://doi.org/10.1111/brv.12215

Holeski, L. M., Jander, G., & Agrawal, A. A. (2012). Transgenerational defense induction and epigenetic inheritance in plants. *Trends in Ecology & Evolution*, *27*(11), 618-626. https://doi.org/10.1016/j.tree.2012.07.011

How to Cite R and R Packages. (s. d.). Consulté 14 octobre 2025, à l'adresse https://ropensci.org/blog/2021/11/16/how-to-cite-r-and-r-packages/

Inácio, V., Santos, R., Prazeres, R., Graça, J., Miguel, C. M., & Morais-Cecílio, L. (2022). Epigenetics at the crossroads of secondary growth regulation. *Frontiers in Plant Science*, *13*. https://doi.org/10.3389/fpls.2022.970342

Jaspers, P., Overmyer, K., Wrzaczek, M., Vainonen, J. P., Blomster, T., Salojärvi, J., Reddy, R. A., & Kangasjärvi, J. (2010). The RST and PARP-like domain containing SRO protein family : Analysis of protein structure, function and conservation in land plants. *BMC Genomics*, *11*(1), 170. https://doi.org/10.1186/1471-2164-11-170

Kakoulidou, I., Avramidou, E. V., Baránek, M., Brunel-Muguet, S., Farrona, S., Johannes, F., Kaiserli, E., Lieberman-Lazarovich, M., Martinelli, F., Mladenov, V., Testillano, P. S., Vassileva, V., & Maury, S. (2021). Epigenetics for Crop Improvement in Times of Global Change. *Biology*, *10*(8), 766. https://doi.org/10.3390/biology10080766

Krueger, F., James, F., Ewels, P., Afyounian, E., Weinstein, M., Schuster-Boeckler, B., Hulselmans, G., & sclamons. (2023). *FelixKrueger/TrimGalore : V0.6.10 - add default decompression path* (Version 0.6.10) [Logiciel]. Zenodo. https://doi.org/10.5281/zenodo.7598955

Kuromori, T., Seo, M., & Shinozaki, K. (2018). ABA Transport and Plant Water Stress Responses. *Trends in Plant Science*, *23*(6), 513-522. https://doi.org/10.1016/j.tplants.2018.04.001

Lafon-Placette, C., Le Gac, A.-L., Chauveau, D., Segura, V., Delaunay, A., Lesage-Descauses, M.-C., Hummel, I., Cohen, D., Jesson, B., Le Thiec, D., Bogeat-Triboulot, M.-B., Brignolas, F., & Maury, S. (2018). Changes in the epigenome and transcriptome of the poplar shoot apical meristem in response to water availability affect preferentially hormone pathways. *Journal of Experimental Botany*, *69*(3), 537-551. https://doi.org/10.1093/jxb/erx409

Lämke, J., & Bäurle, I. (2017). Epigenetic and chromatin-based mechanisms in environmental stress adaptation and stress memory in plants. *Genome Biology*, *18*(1), 124. https://doi.org/10.1186/s13059-017-1263-6

Le Gac, A.-L., Lafon-Placette, C., Chauveau, D., Segura, V., Delaunay, A., Fichot, R., Marron, N., Le Jan, I., Berthelot, A., Bodineau, G., Bastien, J.-C., Brignolas, F., & Maury, S. (2018). Winter-dormant shoot apical meristem in poplar trees shows environmental epigenetic memory. *Journal of Experimental Botany*, *69*(20), 4821-4837. https://doi.org/10.1093/jxb/ery271

Le Gac, A. laure, C, L.-P., A, D., & S, M. (2019). Developmental, genetic and environmental variations of global DNA methylation in the first leaves emerging from the shoot apical meristem in poplar trees. *Plant Signaling & Behavior*, *14*(6), 1596717. https://doi.org/10.1080/15592324.2019.1596717

Leple, J. C., Brasileiro, A. C. M., Michel, M. F., Delmotte, F., & Jouanin, L. (1992). Transgenic poplars : Expression of chimeric genes using four different constructs. *Plant Cell Reports*, *11*(3), 137-141. https://doi.org/10.1007/BF00232166

Liang, D., Zhang, Z., Wu, H., Huang, C., Shuai, P., Ye, C.-Y., Tang, S., Wang, Y., Yang, L., Wang, J., Yin, W., & Xia, X. (2014). Single-base-resolution methylomes of populus trichocarpa reveal the association between DNA methylation and drought stress. *BMC Genetics*, *15*(1), S9. https://doi.org/10.1186/1471-2156-15-S1-S9

Lin, W., Sun, L., Huang, R.-Z., Liang, W., Liu, X., He, H., Fukuda, H., He, X.-Q., & Qian, W. (2020). Active DNA demethylation regulates tracheary element differentiation in Arabidopsis. *Science Advances*, *6*(26), eaaz2963. https://doi.org/10.1126/sciadv.aaz2963

Liu, C., Wang, C., Wang, G., Becker, C., Zaidem, M., & Weigel, D. (2016). Genome-wide analysis of chromatin packing in Arabidopsis thaliana at single-gene resolution. *Genome Research*, *26*(8), 1057-1068. https://doi.org/10.1101/gr.204032.116

Lloyd, J. P. B., & Lister, R. (2022). Epigenome plasticity in plants. *Nature Reviews. Genetics*, *23*(1), 55-68. https://doi.org/10.1038/s41576-021-00407-y

López Sánchez, A., Stassen, J. H. M., Furci, L., Smith, L. M., & Ton, J. (2016). The role of DNA (de)methylation in immune responsiveness of Arabidopsis. *The Plant Journal: For Cell and Molecular Biology*, *88*(3), 361-374. https://doi.org/10.1111/tpj.13252

Love, M. I., Huber, W., & Anders, S. (2014). Moderated estimation of fold change and dispersion for RNA-seq data with DESeq2. *Genome Biology*, *15*(12), 550. https://doi.org/10.1186/s13059-014-0550-8

Luo, Y., Takagi, J., Claus, L. A. N., Zhang, C., Yasuda, S., Hasegawa, Y., Yamaguchi, J., Shan, L., Russinova, E., & Sato, T. (2022). Deubiquitinating enzymes UBP12 and UBP13 stabilize the brassinosteroid receptor BRI1. *EMBO reports*, *23*(4), e53354. https://doi.org/10.15252/embr.202153354

Mader, M., Le Paslier, M.-C., Bounon, R., Bérard, A., Rampant, P. F., Fladung, M., Leplé, J.-C., & Kersten, B. (2016). Whole-genome draft assembly of *Populus tremula* x *P. alba* clone INRA 717-1B4. *Silvae Genetica*, *65*(2), 74-79. https://doi.org/10.1515/sg-2016-0019

Mähönen, A. P., Bishopp, A., Higuchi, M., Nieminen, K. M., Kinoshita, K., Törmäkangas, K., Ikeda, Y., Oka, A., Kakimoto, T., & Helariutta, Y. (2006). Cytokinin Signaling and Its Inhibitor AHP6 Regulate Cell Fate During Vascular Development. *Science*, *311*(5757), 94-98. https://doi.org/10.1126/science.1118875

Mauch-Mani, B., Baccelli, I., Luna, E., & Flors, V. (2017). Defense Priming : An Adaptive Part of Induced Resistance. *Annual Review of Plant Biology*, *68*(Volume 68, 2017), 485-512. https://doi.org/10.1146/annurev-arplant-042916-041132

Maury, S., Sow, M. D., Le Gac, A.-L., Genitoni, J., Lafon-Placette, C., & Mozgova, I. (2019). Phytohormone and Chromatin Crosstalk : The Missing Link For Developmental Plasticity? *Frontiers in Plant Science*, *10*, 395. https://doi.org/10.3389/fpls.2019.00395

McDowell, N. G., Sapes, G., Pivovaroff, A., Adams, H. D., Allen, C. D., Anderegg, W. R. L., Arend, M., Breshears, D. D., Brodribb, T., Choat, B., Cochard, H., De Cáceres, M., De Kauwe, M. G., Grossiord, C., Hammond, W. M., Hartmann, H., Hoch, G., Kahmen, A., Klein, T., … Xu, C. (2022). Mechanisms of woody-plant mortality under rising drought, CO2 and vapour pressure deficit. *Nature Reviews Earth & Environment*, *3*(5), 294-308. https://doi.org/10.1038/s43017-022-00272-1

Mhiri, C., Borges, F., & Grandbastien, M.-A. (2022). Specificities and Dynamics of Transposable Elements in Land Plants. *Biology*, *11*(4), 488. https://doi.org/10.3390/biology11040488

Muyle, A. M., Seymour, D. K., Lv, Y., Huettel, B., & Gaut, B. S. (2022). Gene Body Methylation in Plants : Mechanisms, Functions, and Important Implications for Understanding Evolutionary Processes. *Genome Biology and Evolution*, *14*(4), evac038. https://doi.org/10.1093/gbe/evac038

Nicotra, A. B., Atkin, O. K., Bonser, S. P., Davidson, A. M., Finnegan, E. J., Mathesius, U., Poot, P., Purugganan, M. D., Richards, C. L., Valladares, F., & van Kleunen, M. (2010). Plant phenotypic plasticity in a changing climate. *Trends in Plant Science*, *15*(12), 684-692. https://doi.org/10.1016/j.tplants.2010.09.008

Niederhuth, C. E., Bewick, A. J., Ji, L., Alabady, M. S., Kim, K. D., Li, Q., Rohr, N. A., Rambani, A., Burke, J. M., Udall, J. A., Egesi, C., Schmutz, J., Grimwood, J., Jackson, S. A., Springer, N. M., & Schmitz, R. J. (2016). Widespread natural variation of DNA methylation within angiosperms. *Genome Biology*, *17*(1), 194. https://doi.org/10.1186/s13059-016-1059-0

Nieminen, K., Blomster, T., Helariutta, Y., & Mähönen, A. P. (2015). Vascular Cambium Development. *The Arabidopsis Book / American Society of Plant Biologists*, *13*, e0177. https://doi.org/10.1199/tab.0177

Nieminen, K., Immanen, J., Laxell, M., Kauppinen, L., Tarkowski, P., Dolezal, K., Tähtiharju, S., Elo, A., Decourteix, M., Ljung, K., Bhalerao, R., Keinonen, K., Albert, V. A., & Helariutta, Y. (2008). Cytokinin signaling regulates cambial development in poplar. *Proceedings of the National Academy of Sciences*, *105*(50), 20032-20037. https://doi.org/10.1073/pnas.0805617106

Ojolo, S. P., Cao, S., Priyadarshani, S. V. G. N., Li, W., Yan, M., Aslam, M., Zhao, H., & Qin, Y. (2018). Regulation of Plant Growth and Development : A Review From a Chromatin Remodeling Perspective. *Frontiers in Plant Science*, *9*, 1232. https://doi.org/10.3389/fpls.2018.01232

Park, S.-H., Jeong, J. S., Zhou, Y., Binte Mustafa, N. F., & Chua, N.-H. (2022). Deubiquitination of BES1 by UBP12/UBP13 promotes brassinosteroid signaling and plant growth. *Plant Communications*, *3*(5), 100348. https://doi.org/10.1016/j.xplc.2022.100348

Patro, R., Duggal, G., Love, M. I., Irizarry, R. A., & Kingsford, C. (2017). Salmon provides fast and bias-aware quantification of transcript expression. *Nature Methods*, *14*(4), 417-419. https://doi.org/10.1038/nmeth.4197

Peirats-Llobet, M., Han, S.-K., Gonzalez-Guzman, M., Jeong, C. W., Rodriguez, L., Belda-Palazon, B., Wagner, D., & Rodriguez, P. L. (2016). A Direct Link between Abscisic Acid Sensing and the Chromatin-Remodeling ATPase BRAHMA via Core ABA Signaling Pathway Components. *Molecular Plant*, *9*(1), 136-147. https://doi.org/10.1016/j.molp.2015.10.003

Planas-Riverola, A., Gupta, A., Betegón-Putze, I., Bosch, N., Ibañes, M., & Caño-Delgado, A. I. (2019). Brassinosteroid signaling in plant development and adaptation to stress. *Development (Cambridge, England)*, *146*(5), dev151894. https://doi.org/10.1242/dev.151894

Plomion, C., Aury, J.-M., Amselem, J., Leroy, T., Murat, F., Duplessis, S., Faye, S., Francillonne, N., Labadie, K., Le Provost, G., Lesur, I., Bartholomé, J., Faivre-Rampant, P., Kohler, A., Leplé, J.-C., Chantret, N., Chen, J., Diévart, A., Alaeitabar, T., … Salse, J. (2018). Oak genome reveals facets of long lifespan. *Nature Plants*, *4*(7), 440-452. https://doi.org/10.1038/s41477-018-0172-3

Ramakrishnan, M., Satish, L., Kalendar, R., Narayanan, M., Kandasamy, S., Sharma, A., Emamverdian, A., Wei, Q., & Zhou, M. (2022). Correction : Ramakrishnan et al. The Dynamism of Transposon Methylation for Plant Development and Stress Adaptation. Int. J. Mol. Sci. 2021, 22, 11387. *International Journal of Molecular Sciences*, *23*(22), 14107. https://doi.org/10.3390/ijms232214107

Richards, E. J. (2006). Inherited epigenetic variation—Revisiting soft inheritance. *Nature Reviews Genetics*, *7*(5), 395-401. https://doi.org/10.1038/nrg1834

Rogier, O., Chateigner, A., Lesage-Descauses, M.-C., Mandin, C., Brunaud, V., Caius, J., Soubigou-Taconnat, L., Almeida-Falcon, J., Bastien, C., Benoit, V., Bodineau, G., Boizot, N., Buret, C., Charpentier, J.-P., Déjardin, A., Delaunay, A., Fichot, R., Laine Prade, V., Laurans, F., … Segura, V. (2023). RNAseq based variant dataset in a black poplar association panel. *BMC Research Notes*, *16*(1), 248. https://doi.org/10.1186/s13104-023-06521-w

Ruzicka, K., Ursache, R., & Hejátko, J. (2015, mars 23). *Xylem development – from the cradle to the grave*. https://nph.onlinelibrary.wiley.com/doi/10.1111/nph.13383

Shen, S., Park, J. W., Lu, Z., Lin, L., Henry, M. D., Wu, Y. N., Zhou, Q., & Xing, Y. (2014). rMATS : Robust and flexible detection of differential alternative splicing from replicate RNA-Seq data. *Proceedings of the National Academy of Sciences of the United States of America*, *111*(51), E5593-5601. https://doi.org/10.1073/pnas.1419161111

Shen, X., Jonge, J. D., Forsberg, S. K. G., Pettersson, M. E., Sheng, Z., Hennig, L., & Carlborg, Ö. (2014). Natural CMT2 Variation Is Associated With Genome-Wide Methylation Changes and Temperature Seasonality. *PLOS Genetics*, *10*(12), e1004842. https://doi.org/10.1371/journal.pgen.1004842

Smetana, O., Mäkilä, R., Lyu, M., Amiryousefi, A., Sánchez Rodríguez, F., Wu, M.-F., Solé-Gil, A., Leal Gavarrón, M., Siligato, R., Miyashima, S., Roszak, P., Blomster, T., Reed, J. W., Broholm, S., & Mähönen, A. P. (2019). High levels of auxin signalling define the stem-cell organizer of the vascular cambium. *Nature*, *565*(7740), 485-489. https://doi.org/10.1038/s41586-018-0837-0

Sow, M. D., Le Gac, A.-L., Fichot, R., Lanciano, S., Delaunay, A., Le Jan, I., Lesage-Descauses, M.-C., Citerne, S., Caius, J., Brunaud, V., Soubigou-Taconnat, L., Cochard, H., Segura, V., Chaparro, C., Grunau, C., Daviaud, C., Tost, J., Brignolas, F., Strauss, S. H., … Maury, S. (2021). RNAi suppression of DNA methylation affects the drought stress response and genome integrity in transgenic poplar. *The New Phytologist*, *232*(1), 80-97. https://doi.org/10.1111/nph.17555

Sow, M. D., Rogier, O., Lesur, I., Daviaud, C., Mardoc, E., Sanou, E., Duvaux, L., Civan, P., Delaunay, A., Descauses, M.-C. L.-, Benoit, V., Le-Jan, I., Buret, C., Besse, C., Durufle, H., Fichot, R., Le-Provost, G., Guichoux, E., Boury, C., … Salse, J. (2023). *Epigenetic Variation in Tree Evolution : A case study in black poplar (Populus nigra)* (p. 2023.07.16.549253). bioRxiv. https://doi.org/10.1101/2023.07.16.549253

Steinbach, D., Alaux, M., Amselem, J., Choisne, N., Durand, S., Flores, R., Keliet, A.-O., Kimmel, E., Lapalu, N., Luyten, I., Michotey, C., Mohellibi, N., Pommier, C., Reboux, S., Valdenaire, D., Verdelet, D., & Quesneville, H. (2013). GnpIS : An information system to integrate genetic and genomic data from plants and fungi. *Database: The Journal of Biological Databases and Curation*, *2013*, bat058. https://doi.org/10.1093/database/bat058

Stroud, H., Do, T., Du, J., Zhong, X., Feng, S., Johnson, L., Patel, D. J., & Jacobsen, S. E. (2014). Non-CG methylation patterns shape the epigenetic landscape in Arabidopsis. *Nature Structural & Molecular Biology*, *21*(1), 64-72. https://doi.org/10.1038/nsmb.2735

Talarico, E., Zambelli, A., Araniti, F., Greco, E., Chiappetta, A., & Bruno, L. (2024). Unravelling the Epigenetic Code : DNA Methylation in Plants and Its Role in Stress Response. *Epigenomes*, *8*(3), 30. https://doi.org/10.3390/epigenomes8030030

Teotia, S., & Lamb, R. S. (2011). RCD1 and SRO1 are necessary to maintain meristematic fate in Arabidopsis thaliana. *Journal of Experimental Botany*, *62*(3), 1271-1284. https://doi.org/10.1093/jxb/erq363

Teotia, S., Muthuswamy, S., & Lamb, R. (2009, octobre 21). *Full article : Radical-induced cell death1 and similar to RCD one1 and the stress-induced morphogenetic response*. https://www.tandfonline.com/doi/full/10.4161/psb.5.2.10400

Tong, H., Xiao, Y., Liu, D., Gao, S., Liu, L., Yin, Y., Jin, Y., Qian, Q., & Chu, C. (2014). Brassinosteroid Regulates Cell Elongation by Modulating Gibberellin Metabolism

in Rice. *The Plant Cell*, *26*(11), 4376-4393. https://doi.org/10.1105/tpc.114.132092

Trincado, J. L., Entizne, J. C., Hysenaj, G., Singh, B., Skalic, M., Elliott, D. J., & Eyras, E. (2018). SUPPA2 : Fast, accurate, and uncertainty-aware differential splicing analysis across multiple conditions. *Genome Biology*, *19*(1), 40. https://doi.org/10.1186/s13059-018-1417-1

Trontin, J.-F., Raschke, J., & Rupps, A. (2021). Tree 'memory' : New insights on temperature-induced priming effects during early embryogenesis. *Tree Physiology*, *41*(6), 906-911. https://doi.org/10.1093/treephys/tpaa150

Trontin, J.-F., Sow, M. D., Delaunay, A., Modesto, I., Teyssier, C., Reymond, I., Canlet, F., Boizot, N., Le Metté, C., Gibert, A., Chaparro, C., Daviaud, C., Tost, J., Miguel, C., Lelu-Walter, M.-A., & Maury, S. (2024). Epigenetic memory of temperature sensed during somatic embryo maturation in 2-year-old maritime pine trees. *Plant Physiology*, kiae600. https://doi.org/10.1093/plphys/kiae600

Vanden Broeck, A., Meese, T., Verschelde, P., Cox, K., Heinze, B., Deforce, D., De Meester, E., & Van Nieuwerburgh, F. (2024). Genome-wide methylome stability and parental effects in the worldwide distributed Lombardy poplar. *BMC Biology*, *22*(1), 30. https://doi.org/10.1186/s12915-024-01816-1

Vigneaud, J., Kohler, A., Sow, M. D., Delaunay, A., Fauchery, L., Guinet, F., Daviaud, C., Barry, K. W., Keymanesh, K., Johnson, J., Singan, V., Grigoriev, I., Fichot, R., Conde, D., Perales, M., Tost, J., Martin, F. M., Allona, I., Strauss, S. H., … Maury, S. (2023). DNA hypomethylation of the host tree impairs interaction with mutualistic ectomycorrhizal fungus. *New Phytologist*, *238*(6), 2561-2577. https://doi.org/10.1111/nph.18734

Vongs, A., Kakutani, T., Martienssen, R. A., & Richards, E. J. (1993). Arabidopsis thaliana DNA methylation mutants. *Science (New York, N.Y.)*, *260*(5116), 1926-1928. https://doi.org/10.1126/science.8316832

Wang, X., Hu, L., Wang, X., Li, N., Xu, C., Gong, L., & Liu, B. (2016). DNA Methylation Affects Gene Alternative Splicing in Plants : An Example from Rice. *Molecular Plant*, *9*(2), 305-307. https://doi.org/10.1016/j.molp.2015.09.016

Westerband, A. C., Funk, J. L., & Barton, K. E. (2021). Intraspecific trait variation in plants : A renewed focus on its role in ecological processes. *Annals of Botany*, *127*(4), 397-410. https://doi.org/10.1093/aob/mcab011

Wilkins, O., Waldron, L., Nahal, H., Provart, N. J., & Campbell, M. M. (2009). Genotype and time of day shape the Populus drought response. *The Plant Journal*, *60*(4), 703-715. https://doi.org/10.1111/j.1365-313X.2009.03993.x

Wybouw, B., Zhang, X., & Mähönen, A. P. (2024). Vascular cambium stem cells : Past, present and future. *New Phytologist*, *243*(3), 851-865. https://doi.org/10.1111/nph.19897

Xie, G., Du, X., Hu, H., & Du, J. (2025). *Molecular Mechanisms Underlying the Establishment, Maintenance, and Removal of DNA Methylation in Plants*. https://doi.org/10.1146/annurev-arplant-083123-054357

Xiong, M., Feng, G.-N., Gao, Q., Zhang, C.-Q., Li, Q.-F., Liu, Q.-Q., Xiong, M., Feng, G.-N., Gao, Q., Zhang, C.-Q., Li, Q.-F., & Liu, Q.-Q. (2022). Brassinosteroid regulation in rice seed biology. *Seed Biology*, *1*(1), 1-9. https://doi.org/10.48130/SeedBio-2022-0002

Xu, G., & Law, J. A. (2024). Loops, crosstalk, and compartmentalization : It takes many layers to regulate DNA methylation. *Current Opinion in Genetics & Development*, *84*, 102147. https://doi.org/10.1016/j.gde.2023.102147

Yamamuro, C., Zhu, J.-K., & Yang, Z. (2016). Epigenetic Modifications and Plant Hormone Action. *Molecular Plant*, *9*(1), 57-70. https://doi.org/10.1016/j.molp.2015.10.008

Yang, J., & Johannes, F. (2025). DNA methylation dynamics in the shoot apical meristem. *Journal of Experimental Botany*, *76*(9), 2478-2486. https://doi.org/10.1093/jxb/eraf024

Zhang, H., Lang, Z., & Zhu, J.-K. (2018). Dynamics and function of DNA methylation in plants. *Nature Reviews. Molecular Cell Biology*, *19*(8), 489-506. https://doi.org/10.1038/s41580-018-0016-z

Zhang, S., Hu, N., & Yu, F. (2024). Insights into a functional model of key deubiquitinases UBP12/13 in plants. *New Phytologist*, *242*(2), 424-430. https://doi.org/10.1111/nph.19639

Zhang, X., Yazaki, J., Sundaresan, A., Cokus, S., Chan, S. W.-L., Chen, H., Henderson, I. R., Shinn, P., Pellegrini, M., Jacobsen, S. E., & Ecker, J. R. (2006). Genome-wide high-resolution mapping and functional analysis of DNA methylation in arabidopsis. *Cell*, *126*(6), 1189-1201. https://doi.org/10.1016/j.cell.2006.08.003

Zhang, Y., Liu, C., Cheng, H., Tian, S., Liu, Y., Wang, S., Zhang, H., Saqib, M., Wei, H., & Wei, Z. (2020). DNA methylation and its effects on gene expression during primary to secondary growth in poplar stems. *BMC Genomics*, *21*(1), 498. https://doi.org/10.1186/s12864-020-06902-6

Zhao, B., Liu, Q., Wang, B., & Yuan, F. (2021). Roles of Phytohormones and Their Signaling Pathways in Leaf Development and Stress Responses. *Journal of Agricultural and Food Chemistry*, *69*(12), 3566-3584. https://doi.org/10.1021/acs.jafc.0c07908

Zhou, W., Wang, M., Wang, L., Liu, Y., Tian, Z., Xie, L., & Wang, Y. (2025). Epigenetics in Plant Response to Climate Change. *Biology*, *14*(6), 631. https://doi.org/10.3390/biology14060631

Zhou, Y., Zhou, B., Pache, L., Chang, M., Khodabakhshi, A. H., Tanaseichuk, O., Benner, C., & Chanda, S. K. (2019). Metascape provides a biologist-oriented resource for the analysis of systems-level datasets. *Nature Communications*, *10*(1), 1523. https://doi.org/10.1038/s41467-019-09234-6

Zhu, R., Shevchenko, O., Ma, C., Maury, S., Freitag, M., & Strauss, S. H. (2013). Poplars with a PtDDM1-RNAi transgene have reduced DNA methylation and show aberrant post-dormancy morphology. *Planta*, *237*(6), 1483-1493. https://doi.org/10.1007/s00425-013-1858-4

Zhu, R., Xue, Y., & Qian, W. (2025). Molecular mechanisms and biological functions of active DNA demethylation in plants. *Epigenetics & Chromatin*, *18*(1), 41. https://doi.org/10.1186/s13072-025-00605-6

Figure 1

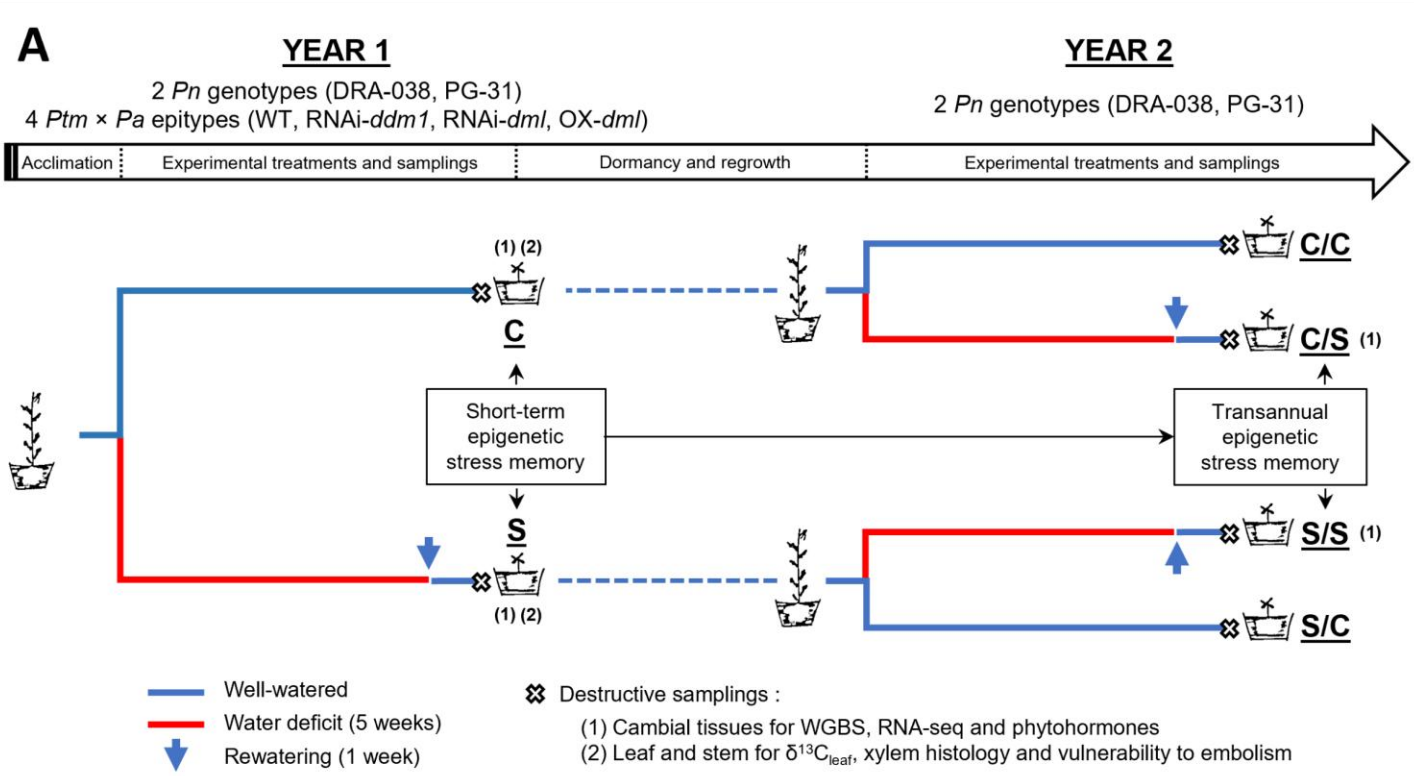
A
YEAR 1
2 Pn genotypes (DRA-038, PG-31)
4 Ptm × Pa epitypes (WT, RNAi-ddm1, RNAi-dml, OX-dml)
YEAR 2
2 Pn genotypes (DRA-038, PG-31)
Acclimation
Experimental treatments and samplings
Dormancy and regrowth
Experimental treatments and samplings
(1) (2)
C
Short-term epigenetic stress memory
S
(1) (2)
C/C
C/S (1)
Transannual epigenetic stress memory
S/S (1)
S/C
Well-watered
Water deficit (5 weeks)
Rewatering (1 week)
Destructive samplings :
(1) Cambial tissues for WGBS, RNA-seq and phytohormones
(2) Leaf and stem for δ13Cleaf, xylem histology and vulnerability to embolism

B

C

Figure 2

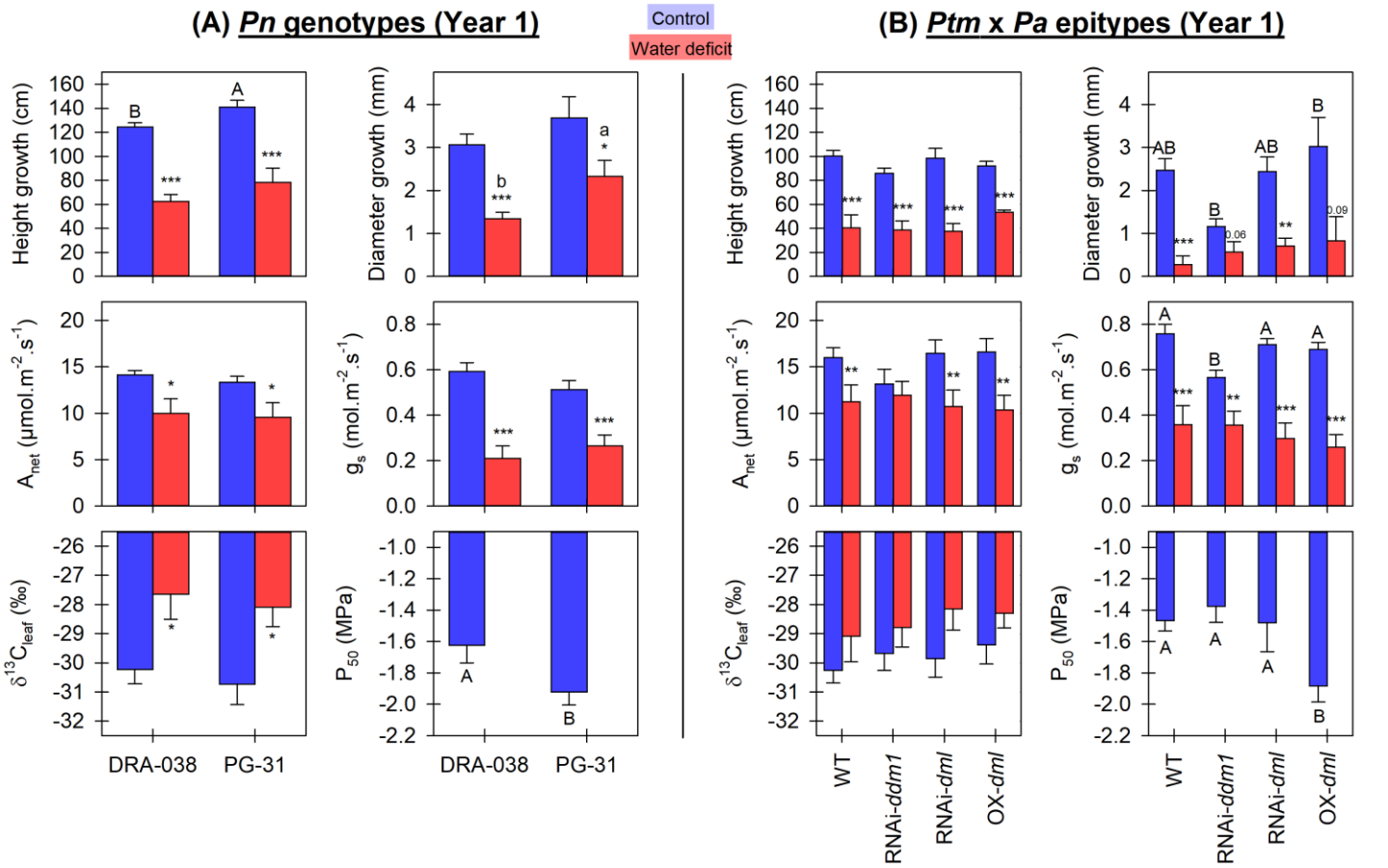

Figure 3

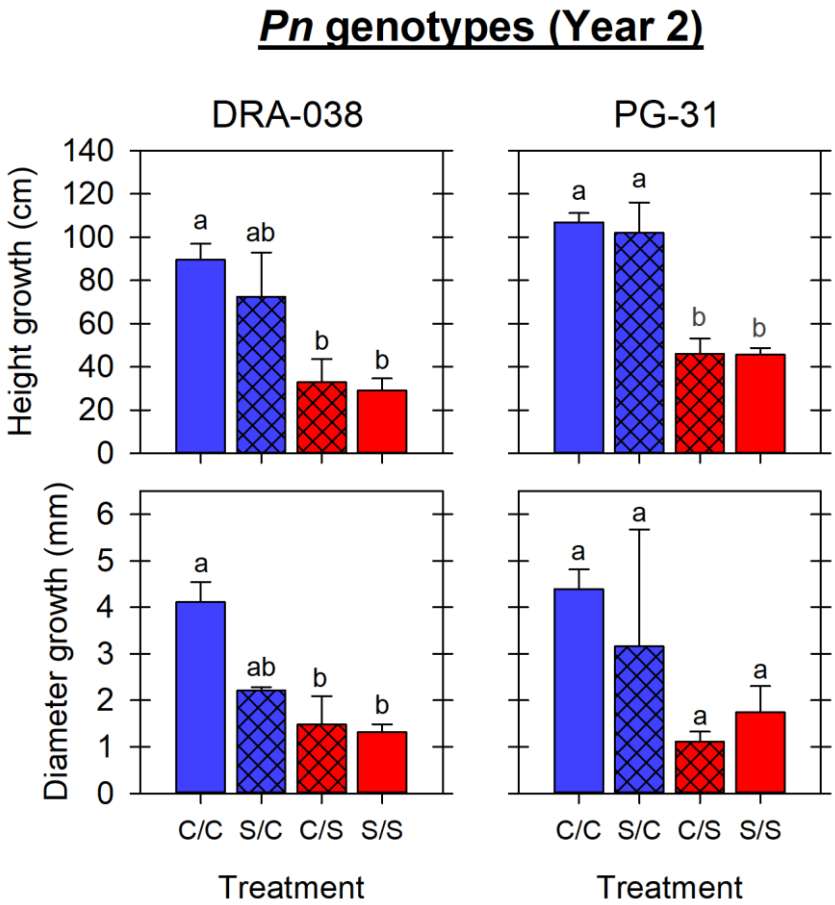

Figure 4

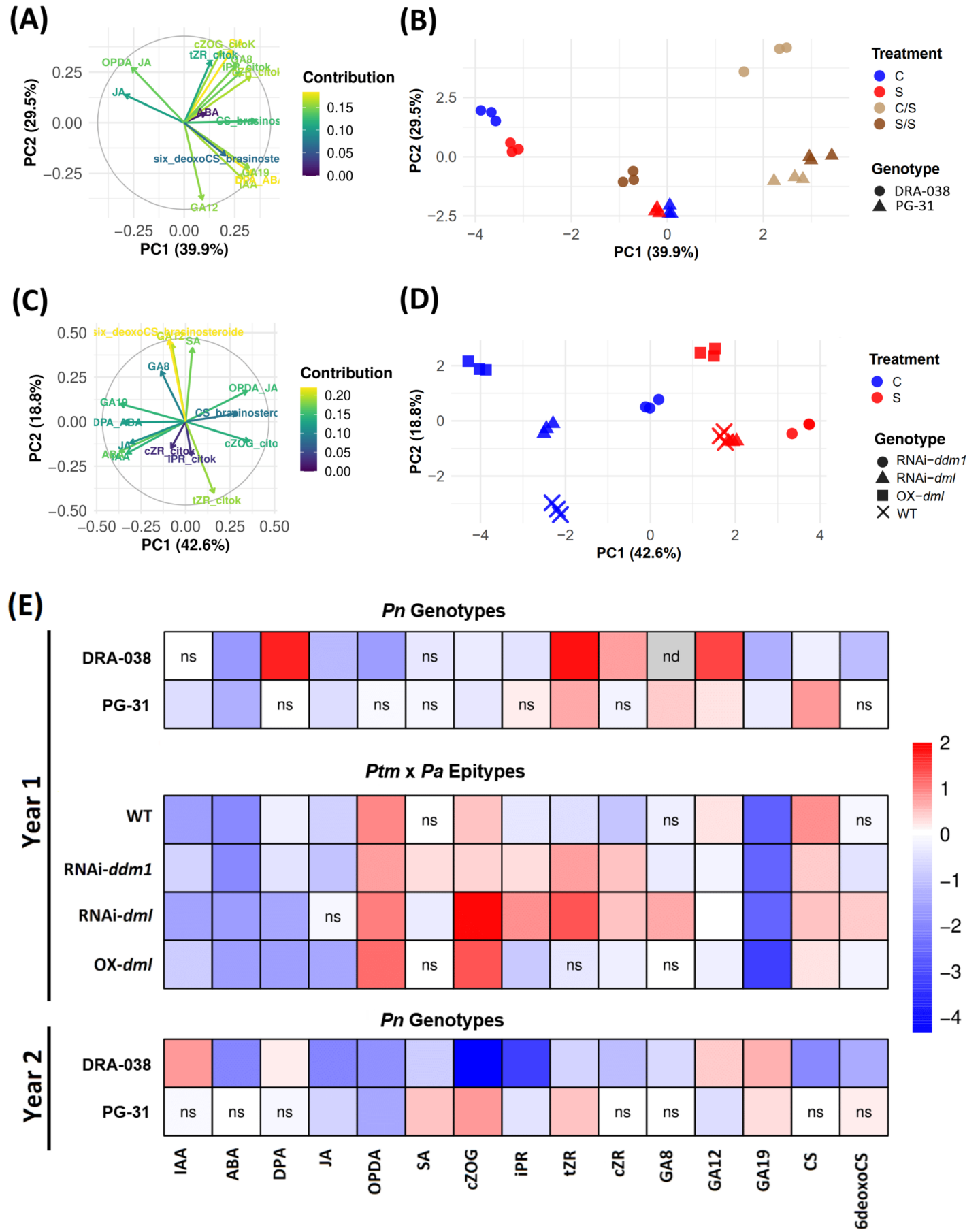
(A)
PC2 (29.5%)
PC1 (39.9%)
Contribution
0.15
0.10
0.05
0.00
OPDA_JA
JA
ABA
GA12
(B)
PC2 (29.5%)
PC1 (39.9%)
Treatment
C
S
C/S
S/S
Genotype
DRA-038
PG-31
(C)
PC2 (18.8%)
PC1 (42.6%)
Contribution
0.20
0.15
0.10
0.05
0.00
GA8
SA
OPDA_JA
GA19
DPA_ABA
cZR_citok
iPR_citok
tZR_citok
(D)
PC2 (18.8%)
PC1 (42.6%)
Treatment
C
S
Genotype
RNAi-ddm1
RNAi-dml
OX-dml
WT
(E)
Pn Genotypes
Ptm x Pa Epitypes
Pn Genotypes
Year 1
Year 2
DRA-038
PG-31
WT
RNAi-ddm1
RNAi-dml
OX-dml
IAA
ABA
DPA
JA
OPDA
SA
cZOG
iPR
tZR
cZR
GA8
GA12
GA19
CS
6deoxoCS
ns
nd

Figure 5

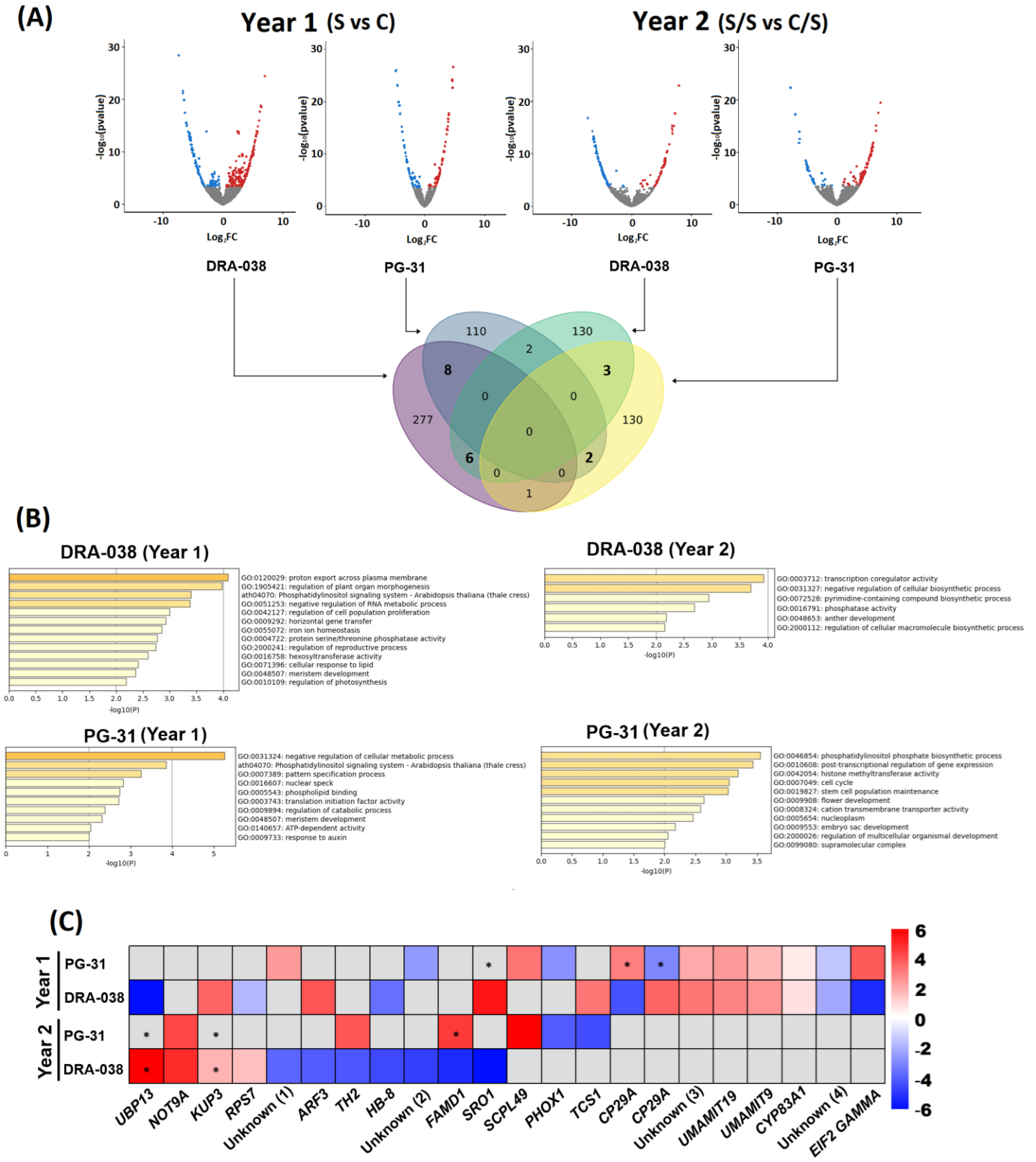
(A)
Year 1 (S vs C)
Year 2 (S/S vs C/S)
-log10(pvalue)
Log2FC
DRA-038
PG-31
DRA-038
PG-31
110
130
2
8
3
0
0
277
130
0
6
2
0
0
1
(B)
DRA-038 (Year 1)
GO:0120029: proton export across plasma membrane
GO:1905421: regulation of plant organ morphogenesis
ath04070: Phosphatidylinositol signaling system - Arabidopsis thaliana (thale cress)
GO:0051253: negative regulation of RNA metabolic process
GO:0042127: regulation of cell population proliferation
GO:0009292: horizontal gene transfer
GO:0055072: iron ion homeostasis
GO:0004722: protein serine/threonine phosphatase activity
GO:2000241: regulation of reproductive process
GO:0016758: hexosyltransferase activity
GO:0071396: cellular response to lipid
GO:0048507: meristem development
GO:0010109: regulation of photosynthesis
-log10(P)
DRA-038 (Year 2)
GO:0003712: transcription coregulator activity
GO:0031327: negative regulation of cellular biosynthetic process
GO:0072528: pyrimidine-containing compound biosynthetic process
GO:0016791: phosphatase activity
GO:0048653: anther development
GO:2000112: regulation of cellular macromolecule biosynthetic process
-log10(P)
PG-31 (Year 1)
GO:0031324: negative regulation of cellular metabolic process
ath04070: Phosphatidylinositol signaling system - Arabidopsis thaliana (thale cress)
GO:0007389: pattern specification process
GO:0016607: nuclear speck
GO:0005543: phospholipid binding
GO:0003743: translation initiation factor activity
GO:0009894: regulation of catabolic process
GO:0048507: meristem development
GO:0140657: ATP-dependent activity
GO:0009733: response to auxin
-log10(P)
PG-31 (Year 2)
GO:0046854: phosphatidylinositol phosphate biosynthetic process
GO:0010608: post-transcriptional regulation of gene expression
GO:0042054: histone methyltransferase activity
GO:0007049: cell cycle
GO:0019827: stem cell population maintenance
GO:0009908: flower development
GO:0008324: cation transmembrane transporter activity
GO:0005654: nucleoplasm
GO:0009553: embryo sac development
GO:2000026: regulation of multicellular organismal development
GO:0099080: supramolecular complex
-log10(P)
(C)
Year 1
PG-31
DRA-038
Year 2
PG-31
DRA-038
UBP13
NOT9A
KUP3
RPS7
Unknown (1)
ARF3
TH2
HB-8
Unknown (2)
FAMD1
SRO1
SCPL49
PHOX1
TCS1
CP29A
CP29A
Unknown (3)
UMAMIT19
UMAMIT9
CYP83A1
Unknown (4)
EIF2 GAMMA
6
4
2
0
-2
-4
-6

Figure 6

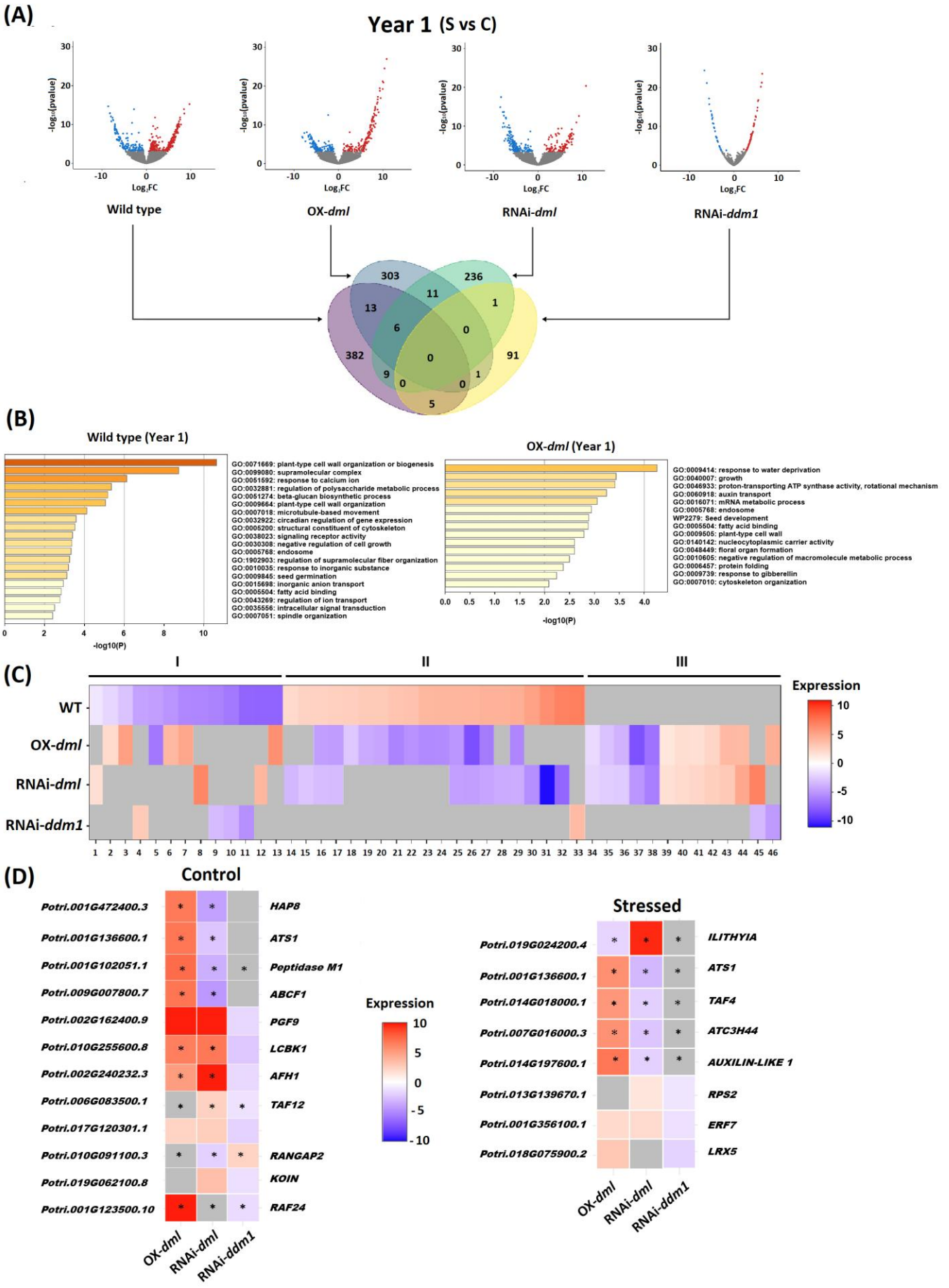
(A)
Year 1 (S vs C)
Wild type
OX-dml
RNAi-dml
RNAi-ddm1
303
236
11
13
1
6
0
382
0
91
9
0
1
0
5
(B)
Wild type (Year 1)
GO:0071669: plant-type cell wall organization or biogenesis
GO:0099080: supramolecular complex
GO:0051592: response to calcium ion
GO:0032881: regulation of polysaccharide metabolic process
GO:0051274: beta-glucan biosynthetic process
GO:0009664: plant-type cell wall organization
GO:0007018: microtubule-based movement
GO:0032922: circadian regulation of gene expression
GO:0005200: structural constituent of cytoskeleton
GO:0038023: signaling receptor activity
GO:0030308: negative regulation of cell growth
GO:0005768: endosome
GO:1902903: regulation of supramolecular fiber organization
GO:0010035: response to inorganic substance
GO:0009845: seed germination
GO:0015698: inorganic anion transport
GO:0005504: fatty acid binding
GO:0043269: regulation of ion transport
GO:0035556: intracellular signal transduction
GO:0007051: spindle organization
-log10(P)
OX-dml (Year 1)
GO:0009414: response to water deprivation
GO:0040007: growth
GO:0046933: proton-transporting ATP synthase activity, rotational mechanism
GO:0060918: auxin transport
GO:0016071: mRNA metabolic process
GO:0005768: endosome
WP2279: Seed development
GO:0005504: fatty acid binding
GO:0009505: plant-type cell wall
GO:0140142: nucleocytoplasmic carrier activity
GO:0048449: floral organ formation
GO:0010605: negative regulation of macromolecule metabolic process
GO:0006457: protein folding
GO:0009739: response to gibberellin
GO:0007010: cytoskeleton organization
-log10(P)
(C)
I
II
III
WT
OX-dml
RNAi-dml
RNAi-ddm1
Expression
(D)
Control
Potri.001G472400.3 HAP8
Potri.001G136600.1 ATS1
Potri.001G102051.1 Peptidase M1
Potri.009G007800.7 ABCF1
Potri.002G162400.9 PGF9
Potri.010G255600.8 LCBK1
Potri.002G240232.3 AFH1
Potri.006G083500.1 TAF12
Potri.017G120301.1
Potri.010G091100.3 RANGAP2
Potri.019G062100.8 KOIN
Potri.001G123500.10 RAF24
OX-dml
RNAi-dml
RNAi-ddm1
Expression
Stressed
Potri.019G024200.4 ILITHYIA
Potri.001G136600.1 ATS1
Potri.014G018000.1 TAF4
Potri.007G016000.3 ATC3H44
Potri.014G197600.1 AUXILIN-LIKE 1
Potri.013G139670.1 RPS2
Potri.001G356100.1 ERF7
Potri.018G075900.2 LRX5
OX-dml
RNAi-dml
RNAi-ddm1

Figure 7

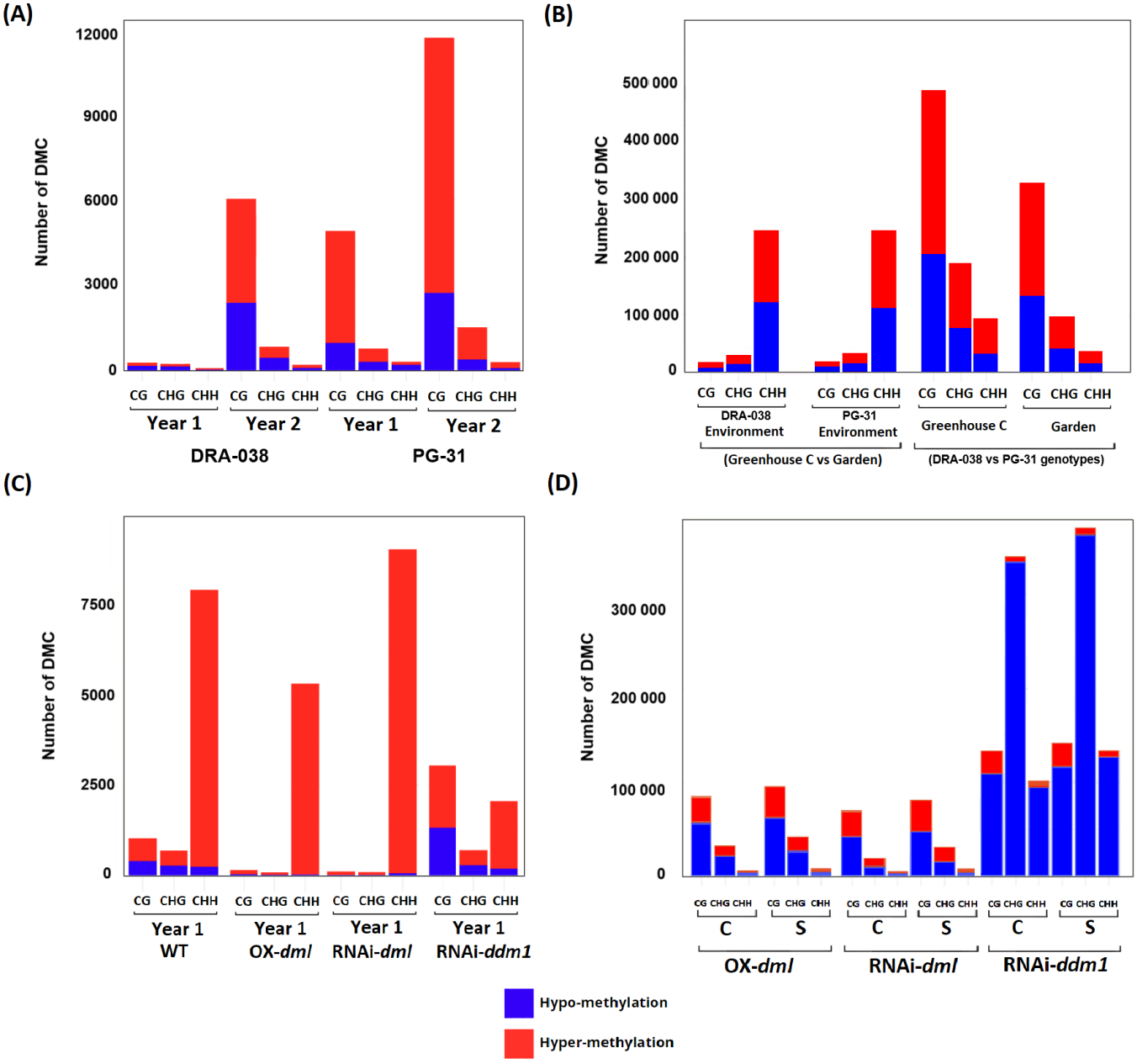
(A)
Number of DMC
12000
9000
6000
3000
0
CG CHG CHH
Year 1
Year 2
DRA-038
PG-31
(B)
500 000
400 000
300 000
200 000
100 000
DRA-038 Environment
PG-31 Environment
Greenhouse C
Garden
(Greenhouse C vs Garden)
(DRA-038 vs PG-31 genotypes)
(C)
7500
5000
2500
WT
OX-dml
RNAi-dml
RNAi-ddm1
(D)
300 000
C
S
OX-dml
RNAi-dml
RNAi-ddm1
Hypo-methylation
Hyper-methylation

Figure 8

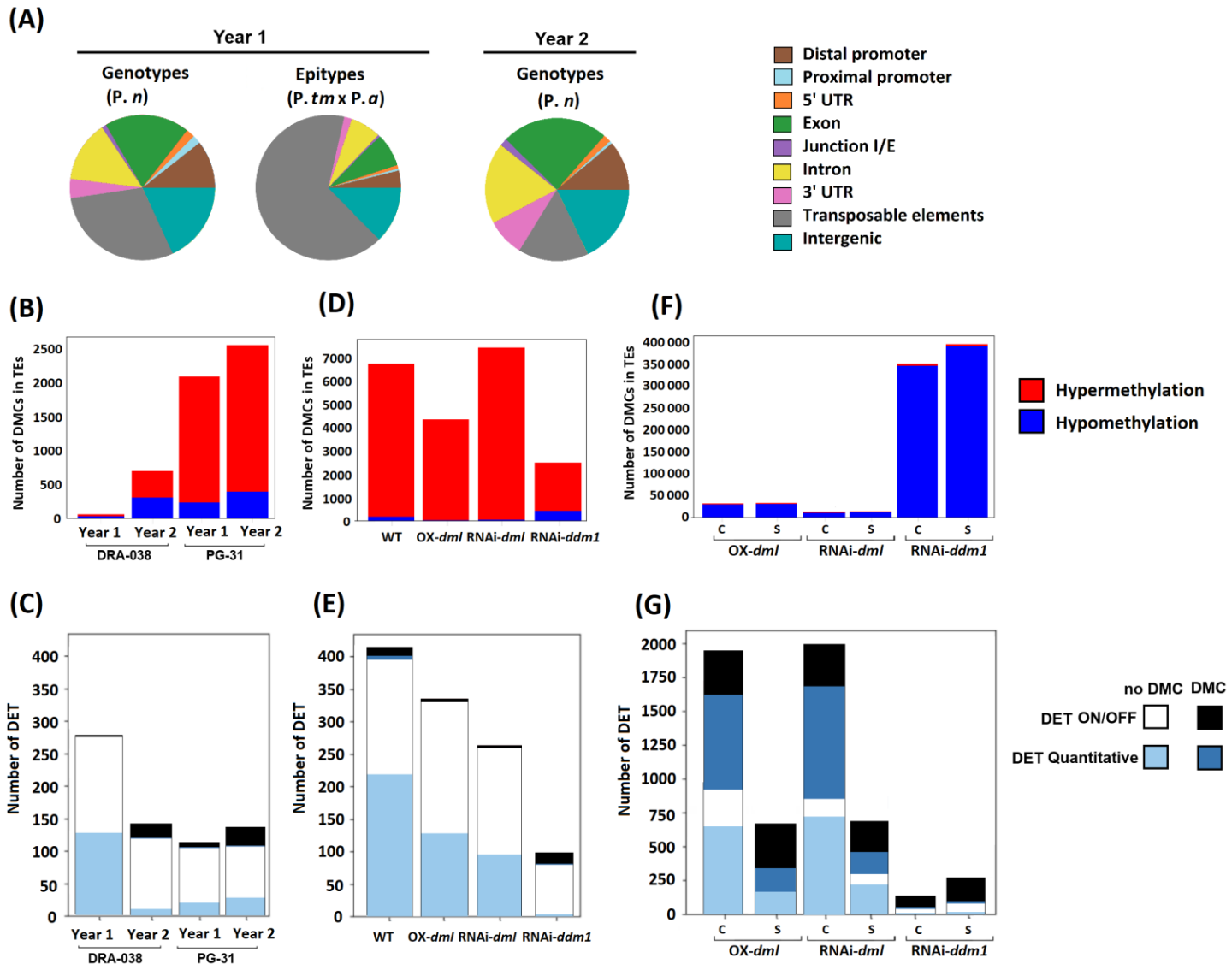
(A)
Year 1
Year 2
Genotypes (P. n)
Epitypes (P. tm x P. a)
Genotypes (P. n)
Distal promoter
Proximal promoter
5' UTR
Exon
Junction I/E
Intron
3' UTR
Transposable elements
Intergenic
(B)
Number of DMCs in TEs
Year 1
Year 2
Year 1
Year 2
DRA-038
PG-31
(D)
Number of DMCs in TEs
WT
OX-dml
RNAi-dml
RNAi-ddm1
(F)
Number of DMCs in TEs
C
S
OX-dml
RNAi-dml
RNAi-ddm1
Hypermethylation
Hypomethylation
(C)
Number of DET
Year 1
Year 2
Year 1
Year 2
DRA-038
PG-31
(E)
Number of DET
WT
OX-dml
RNAi-dml
RNAi-ddm1
(G)
Number of DET
C
S
OX-dml
RNAi-dml
RNAi-ddm1
no DMC
DMC
DET ON/OFF
DET Quantitative

Table 1. Denomination and characteristics of the plant material used in the study

Species	Name	Origin / construction	References
Pn genotypes	DRA-038	South-East France, Dranse river basin	Chateigner et al., 2020; Faivre-Rampant et al., 2016; Gebreselassie et al., 2017; Guet et al., 2015; Rogier et al., 2023; Sow et al., 2023
	PG-31	Central Italy, Paglia river basin	Chateigner et al., 2020; Faivre-Rampant et al., 2016; Gebreselassie et al., 2017; Guet et al., 2015; Rogier et al., 2023; Sow et al., 2023
Ptm × *Pa* epitypes	WT	Wild-type	Leple et al., 1992; Mader et al., 2016
	RNAi-*ddm1*	RNAi-mediated suppression of *PtDDM1*	Sow et al., 2021; Vigneaud et al., 2023; Vongs et al., 1993; Zhu et al., 2013
	RNAi-*dml*	RNAi-mediated suppression of *Pa-DML*	Conde, 2017a; Vigneaud et al., 2023
	OX-*dml*	Overexpression of *Cs-DML*	Conde, 2017b; Vigneaud et al., 2023

(Decreased DNA Methylation 1); *DML (DEMETER-Like DNA demethylase)*; *Cs*, *Castanea sativa; Pa*, *Populus alba*; *Pn, Populus nigra*; *Pt*, *Populus trichocarpa; Ptm, Populus tremula*

Table 2. Overview of the candidate genes found in the study for the genotype analysis

Conditions	Poplar ID	Biological function
Both genotypes Year 1	*Potri.016G090700.3*	***CP29A***, encodes a chloroplast RNA-binding protein that increases in the cold and is repressed by other stressors and ABA.
	Potri.016G090700.2	
	Potri.002G085100.2	***UMAMIT 19***, amino acid exporter, stress response / SA-dep. pathway.
	Potri.003G192500.1	***UMAMIT 9*****,** amino acid exporter, stress response / SA-dep. pathway.
	Potri.002G025425.1	***CYP83A1*****,** encodes a cytochrome p450 enzyme that plays a role in auxin homeostasis.
	Potri.001G129100.7	***EIF2-GAMMA***, protein synthesis initiation factor, essential for growth in stress conditions and development.
	Potri.013G007900.1	Unknown function
	Potri.018G114801.1	Unknown function
	Potri.019G022700.1	***TH2***, a regulation protein that plays a role in vitamin B1 biosynthesis pathway.

DETs (Fig. 5A)	Both genotypes Year 2	*Potri.010G067900.4*	***FAMD1***, encodes a phospholipid synthase. This enzyme plays a key role in the modification of membrane lipids.
		Potri.001G359300.3	***NOT9A***, encodes a RCD1-like protein, a regulator of both developmental and stress responses. Spans the bridge between the RNA-induced silencing complex (RISC) and CCR4-NOT.
	DRA-038 Both Years	*Potri.016G064100.3*	***UBP13***, Ubiquitin-specific protease that plays a role in plant development and stress responses. Positively Regulate MYC2 Levels in Jasmonate Responses
		Potri.006G237500.6	***HB-8***, a protein containing a homeobox domain. Plays a role in control of vein-forming (vascular meristems), striped gene expression by auxin signaling.
		Potri.011G059300.4	***ARFs*** is a transcription factor that plays a role in regulating drought and salinity stress responses in plants.
		Potri.013G138900.3	***RPS7***, a constituent of the small subunit of the ribosomal complex.
		Potri.014G144900.1	***KUP3***, potassium transporter, plays a role in biotic and abiotic stress response and development.
		Potri.003G096700.2	***SRO1*** encodes a transcription factor that is necessary to maintain meristematic fate, mediates stress and developmental responses.

	PG-31 Both Years	*Potri.010G227700.3*	***SCPL49***, encodes a Serine Carboxypeptidase-like 49 identified as a gene associated with adaptation to drought.
		Potri.018G121100.3	***PHOX1*****,** encodes carboxylate clamp TPR potentially interacting with Hsp90/Hsp70 as co-chaperones.
	DRA-038 Year 1	*Potri.003G072300.3*	***FAB1B***, encodes a protein that plays a role in the regulation of membrane recycling, vacuolar pH and homeostatic control of reactive oxygen species (ROS).
		Potri.003G110100.6	***CHR4***, encodes a protein that interacts with TFs involved in floral meristem identity and affects the expression of key floral regulators. Affects H3K27me3 and H3K4me3 levels at a subset of loci in the genome.
		Potri.011G049700.6	***SFR6***, encodes a subunit of the MEDIATOR complex that plays a role in stress response (CBF pathway), auxin mediated gene expression.
		Potri.019G132800.5 *Potri.019G132800.4*	***ATM3***, ABC transporter of the mitochondrion genes have an important function for plant growth (development). Involved in heavy metal resistance.
DSE - DETs	PG-31 Year 1	*Potri.015G036000.2*	***HIP***, encodes a thioredoxin-like disulfide reductase. Interact with HSP70.
		Potri.015G036000.4	

PG-31 Year 2	*Potri.002G133500.4*	***AFR2***, a protein that plays a role in circadian cycle and catalyses H3 deacetylation to repress expression.
	Potri.004G146900.4	***VRN1***, transcription factor required for the methylation of H3. Repression of FLC in vernalized plants.
	Potri.011G169200.9	Unknown function
DRA-038 Year 2	*Potri.016G064100.3*	***UBP13***, Ubiquitin-specific protease that plays a role in plant development and stress responses (JA).

This table contains genes found in the differential expression analyses for genotype. The functions are annotated in more detail in the supplementary table: Sup_table_2. Similar table with genes of interest found in epitypes Sup_table_3. *List of genes with unknown functions identified in the analysis for shared DET in genotypes Year 1: Potri.013G007900.1, Potri.018G114801.1 and AS - DET in PG31 Year 2: Potri.011G169200.9.